Research Square

Preprints are preliminary reports that have not undergone peer review.
They should not be considered conclusive, used to inform clinical practice,
or referenced by the media as validated information.

# LncRNA RP4-694A7.2 promotes non-small cell lung cancer proliferation by activating a YBX1-mediated DEPDC1/Wnt/β-catenin axis

**Dapeng Lu**
Anhui Provincial Hospital
**Jimin Li**
Anhui Provincial Hospital
**Wenqian Dong**
Anhui Provincial Hospital
**Shuang Zhang**
Anhui Provincial Hospital
**Bing He**
Anhui Provincial Hospital
**Maoxin Zhu**
Anhui Provincial Hospital
**Shihao Yu**
Anhui Provincial Hospital
**Peng Luo**
Anhui Provincial Hospital
**Baolong Wang**
wbl1965550163.com

Anhui Provincial Hospital https://orcid.org/0000-0001-7441-2428

**Research Article**

**Keywords:** Non-small cell lung cancer, RP4-694A7.2, Proliferation, YBX1, Ubiquitination, Nuclear import

**Posted Date:** November 5th, 2026

**DOI:** https://doi.org/10.21203/rs.3.rs-11419047/v1

**License:** This work is licensed under a Creative Commons Attribution 4.0 International License.
Read Full License

# LncRNA RP4-694A7.2 promotes non-small cell lung cancer proliferation by activating a YBX1-mediated DEPDC1/Wnt/β-catenin axis

Dapeng Lu[a,b], Jimin Li[a,b], Wenqian Dong[a,b], Shuang Zhang[a,b], Bing He[a,b], Maoxin Zhu[a,b], Shihao Yu[a,b], Peng Luo[a,b,*], Baolong Wang[a,b,*]

[a]Department of Laboratory Medicine, The First Affiliated Hospital of USTC, Division of Life Sciences and Medicine, University of Science and Technology of China, Hefei 230001, China

[b]Core Unit of National Clinical Research Center for Laboratory Medicine, Hefei 230001, China

***Corresponding author's email address**: ahlp1022@163.com (P. Luo), wbl196555@163.com (B. Wang)

## Abstract

**Background** Non-small cell lung cancer (NSCLC) is among the most prevalent malignancies; however, treatment options are limited owing to a paucity of effective therapeutic targets. Although long non-coding RNAs (lncRNAs) are critical regulators of tumor progression, their functional mechanisms and translational potential in NSCLC remain poorly understood. Patient-derived xenograft (PDX) models provide a clinically relevant platform for target discovery

and therapeutic evaluation.

**Methods** By integrating transcriptome screening of NSCLC PDX models with analysis of data from The Cancer Genome Atlas (TCGA), we identified lncRNA RP4-694A7.2 as a key oncogenic target. The expression and clinical relevance of RP4-694A7.2 were assessed using quantitative PCR with reverse transcription and fluorescence in situ hybridization assays. Functional roles were investigated through a series of in vitro assays (CCK-8, colony formation, EdU, and flow cytometry) and experiments using in vivo xenograft models. The underlying molecular mechanisms were dissected using RNA pull-down, mass spectrometry, RNA immunoprecipitation, co-immunoprecipitation, chromatin immunoprecipitation, and luciferase reporter assays. Finally, the therapeutic potential of RP4-694A7.2 was validated in NSCLC PDX models through intratumoral delivery of RP4-694A7.2-targeting small interfering RNAs.

**Results** RP4-694A7.2 was markedly upregulated in NSCLC tissues and cells and promoted NSCLC proliferation by accelerating the G1/S phase transition. Mechanistically, RP4-694A7.2 directly bound to YBX1, suppressing WWP2-mediated K48-linked ubiquitination and proteasomal degradation, thereby enhancing YBX1 stability. Furthermore, RP4-694A7.2 strengthened the YBX1–KPNA2 interaction to facilitate YBX1 nuclear import. Nuclear-accumulated YBX1 subsequently bound to the *DEPDC1* promoter to activate its transcription, leading to activation of the Wnt/β-catenin pathway and upregulation of c-Myc and cyclin D1. Notably, silencing of RP4-694A7.2 using small interfering RNAs markedly

suppressed tumor growth in NSCLC PDX models.

**Conclusions** Our findings show that RP4-694A7.2 promotes NSCLC proliferation through the YBX1/DEPDC1/Wnt/β-catenin axis, indicating that RP4-694A7.2 is a potential therapeutic target for this malignancy.

**Keywords** Non-small cell lung cancer, RP4-694A7.2, Proliferation, YBX1, Ubiquitination, Nuclear import

## Introduction

Non-small cell lung cancer (NSCLC) accounts for approximately 85% of lung cancer cases and represents the leading cause of cancer-related mortality worldwide [1]. It comprises three major histological subtypes: lung adenocarcinoma, lung squamous cell carcinoma (LUSC), and large-cell lung cancer. Despite advances in screening, targeted therapy, and immunotherapy, patients with advanced NSCLC have poor prognoses, with a 5-year survival rate of less than 16% [2]. The limited durability of current therapies can be largely attributed to a lack of effective therapeutic targets and the inevitable emergence of resistance. Therefore, there is an urgent need to identify novel molecular targets that can be translated into effective therapeutic strategies.

Long non-coding RNAs (lncRNAs), which are transcripts longer than 200 nucleotides with limited or no protein-coding capacity [3], have emerged as promising therapeutic targets because of their tissue-specific expression and

their ability to orchestrate oncogenic programs at the transcriptional, post-transcriptional, and post-translational levels [4]. For example, lncRNA SNHG8 promotes myocardial fibrosis by recruiting E2F1 to the *MAD2L1* promoter, indicating its potential as a therapeutic target for cardiac fibrosis [5]. Unlike protein-coding genes, lncRNAs function through modular RNA–protein interactions, making them amenable to oligonucleotide-based therapeutics such as antisense oligonucleotides and small interfering RNAs (siRNAs). For instance, LPCRL drives LUSC cisplatin resistance through the USP15/MIB1/Notch axis, and intratumoral delivery of siRNAs targeting LPCRL has been shown to suppress tumor growth and enhance cisplatin sensitivity in patient-derived xenograft (PDX) models [6]. However, the majority of NSCLC-associated lncRNAs remain functionally and mechanistically uncharacterized, which limits their clinical translation.

PDX models provide a clinically relevant platform for target discovery and therapeutic evaluation because they preserve the histology, genomic heterogeneity, and stromal architecture of primary tumors [7, 8]. The scalability of PDX models enables high-throughput discovery of predictive and prognostic biomarkers, study of tumor heterogeneity, and characterization of target–drug response [9]. In our previous NSCLC PDX models, microarray analysis of lncRNA expression profiles revealed marked transcriptional differences between primary tumors and third-generation (X-3) xenografts [10]. However, whether these differentially expressed lncRNAs drive NSCLC proliferation has remained

unknown, as has whether they can be therapeutically targeted.

Here, by integrating transcriptome screening of NSCLC PDX models with TCGA analysis, we identified marked upregulation of lncRNA RP4-694A7.2 in NSCLC tissues and cells. Functional assays demonstrated that RP4-694A7.2 facilitated NSCLC proliferation in vitro and in vivo. Mechanistically, RP4-694A7.2 directly bound to Y-box binding protein 1 (YBX1), suppressing WW domain-containing E3 ubiquitin protein ligase 2 (WWP2)-mediated ubiquitination and subsequent proteasomal degradation of YBX1, thereby enhancing its stability. Concurrently, RP4-694A7.2 strengthened the interaction between YBX1 and karyopherin subunit alpha 2 (KPNA2), thereby promoting YBX1 nuclear import. Nuclear YBX1 subsequently bound to the DEP domain-containing 1 (*DEPDC1*) promoter to activate its transcription, leading to activation of the Wnt/β-catenin pathway and upregulation of downstream effectors c-Myc and cyclin D1. Notably, siRNA-mediated knockdown of RP4-694A7.2 markedly inhibited tumor growth in NSCLC PDX models. Collectively, our findings demonstrate a key role of the RP4-694A7.2/YBX1/DEPDC1/Wnt/β-catenin axis in driving NSCLC proliferation, highlighting RP4-694A7.2 as a promising therapeutic target.

## Materials and methods

### Patients and specimens

A total of 20 paired tumor tissues and adjacent non-tumor tissues (ANTs) (>5 cm from tumors) from NSCLC patients were obtained from the First Affiliated Hospital

of USTC, Division of Life Sciences and Medicine, University of Science and Technology of China. All procedures were implemented in accordance with the Helsinki Declaration. After collection, tissue samples were immediately frozen in liquid nitrogen.

**Cell lines and cell culture**

SK-MES-1 and HEK293T cell lines were obtained from the Cell Bank of the Chinese Academy of Sciences (Shanghai, China). The NCI-H520, H2170, A549, H1299, and BEAS-2B cell lines were purchased from the American Type Culture Collection (Manassas, VA, USA). We established a primary NSCLC cell line by mincing fresh tumor tissue from surgical resection, digesting it with collagenase, filtering the resulting cell suspension, and collecting cells by centrifugation. SK-MES-1 and BEAS-2B cells were cultured in Dulbecco's modified Eagle medium with 10% fetal bovine serum. NCI-H520, H2170, A549, H1299, HEK293T, and primary cells were cultured in RPMI 1640 medium with 10% fetal bovine serum. All cells were cultured in a humidified incubator at 37 °C with 5% $CO_2$.

**Plasmid and siRNA transfection**

For siRNA transfection, NSCLC cells were transfected using Lipofectamine 2000 (Invitrogen, USA) according to the manufacturer's instructions. The plasmids were transfected into NSCLC cells using Hieff Trans® PEI (Yeasen, China). All siRNA sequences are listed in Supplementary Table S1.

## Quantitative PCR with reverse transcription (RT-qPCR)

Total RNA was extracted using TRIzol (Invitrogen, USA), and cytoplasmic and nuclear RNA was extracted with an RNA Subcellular Isolation Kit (Thermo Fisher Scientific, USA) following the instructions provided. cDNA was synthesized using a PrimeScript RT kit (TaKaRa, Japan), and qPCR was performed using Power SYBR Green Master Mix (Vazyme, China). The mRNA internal controls were GAPDH and U6. Sequences of primers are listed in Supplementary Table S2.

## Western blot

Cells were lysed in RIPA buffer (Bestbio, China) containing phosphatase and protease inhibitors. The protein concentration of cell lysates was determined using a BCA Protein Assay Kit (Beyotime, China). Equal amounts of protein were separated by 10% sodium dodecyl sulfate polyacrylamide gel electrophoresis, transferred to polyvinylidene fluoride membranes (Merck Millipore), blocked with 5% skim milk, and sequentially incubated with primary (4 °C, overnight) and secondary (room temperature, 1.5 h) antibodies. Protein bands were visualized using a BeyoECL Star kit (Beyotime, China). All antibody information is provided in Supplementary Table S3.

## Cell counting kit-8 (CCK8)

Cells were seeded into 96-well plates, followed by addition of 10% CCK-8 solution (Dojindo, Japan) and incubation at 37 °C for 2.5 h. The absorbance was

measured at 490 nm.

**Colony formation**

Transfected cells were seeded in a six-well plate. After approximately 2 weeks, 20% methanol and 0.1% crystal violet were used to fix and stain the colonies, which were then counted manually.

**5-ethynyl-2′-deoxyuridine (EdU) assay**

Following seeding of cells in 12-well plates, an EdU assay was performed according to the manufacturer's instructions (Beyotime, China). Cell nuclei were stained with 4′,6-diamidino-2-phenylindole (DAPI).

**Flow cytometry**

Cell cycle distribution was analyzed by flow cytometry after fixation of cells in 75% ethanol at 4 °C overnight, followed by staining with propidium iodide (PI)/RNase Staining Buffer (BD Biosciences, USA).

**RNA pull-down and mass spectrometry (MS)**

Full-length biotinylated sense and antisense RNA probes for RP4-694A7.2 were refolded and immobilized on streptavidin magnetic beads. Bead-bound RNA was incubated with whole-cell lysate to capture interacting proteins. After stringent washing, bound complexes were eluted and analyzed by western blotting or MS.

**RNA immunoprecipitation (RIP)**

Following cell lysis and DNase treatment, protein lysates were divided into immunoprecipitation (IP), IgG, and input groups. Each sample was incubated overnight at 4 °C with 4 μg of the respective antibody or IgG, then co-incubated with Protein A/G magnetic beads (Thermo Fisher Scientific). After magnetic capture and washing, bead-bound RNA was eluted, purified with TRIzol, and analyzed by RT-qPCR, with expression levels normalized to the input. All antibody information is provided in Supplementary Table S3.

**Co-immunoprecipitation (Co-IP)**

Following cell lysis in IP buffer (30 min on ice), the clarified lysates were immunoprecipitated overnight at 4 °C with 2 μg of antibody. Complexes were captured with Protein A/G magnetic beads, stringently washed, and eluted at 100 °C for 10 min before immunoblotting (IB) analysis.

**Dual-luciferase reporter assay**

Dual-luciferase reporters were constructed based on the vector, wild-type (WT) *DEPDC1* promoter (DEPDC1-WT) or mutant *DEPDC1* promoters (Mut1: -TGTCCCATC-; Mut2: -TGTAACATC-). These reporters were co-transfected with an HA-YBX1 plasmid. Luciferase activity was measured using a commercial kit (Vazyme, China) according to the manufacturer's protocol. The activity of the firefly luciferase reporter was determined by normalization to the Renilla

199 luciferase control.

200

201 **Chromatin immunoprecipitation (ChIP)**

202 ChIP was performed using a SimpleChIP® Kit according to the manufacturer's
203 protocol. Briefly, NSCLC cells were cross-linked with 1% formaldehyde, and
204 chromatin was digested with micrococcal nuclease to 150–900 bp fragments. The
205 sheared chromatin was incubated overnight at 4 °C with anti-YBX1 antibody or
206 IgG, followed by capture with Protein G magnetic beads for 2 h. After cross-link
207 reversal and DNA purification, enrichment of the target sequence (-
208 TGTAACATC- motif in the *DEPDC1* promoter) was quantified by qPCR using
209 specific primer DEPDC1-Mut2-F/R. Primer sequences and antibody information
210 are provided in Supplementary Tables S2 and S3, respectively.

211

212 **RNA-fluorescence in situ hybridization (FISH)**

213 A specific RNA-FISH probe targeting RP4-694A7.2 (RiboBio, China) was used
214 according to the manufacturer's instructions. Briefly, cells were fixed,
215 permeabilized, and hybridized with the probe overnight at 37°C, followed by DAPI
216 counterstaining. The same probe was used for in situ hybridization on NSCLC
217 tissues. Its oligonucleotide sequence was provided by RiboBio.

218

219 **Immunofluorescence (IF)**

220 Cells were fixed with 4% paraformaldehyde for 20 min, permeabilized with 0.5%

Triton X-100/PBS (20 min, room temperature), and blocked with 1% bovine serum albumin for 30 min. They were then incubated with primary antibody overnight at 4 °C, followed by incubation with the appropriate secondary antibody for 30 min at 37 °C in the dark. Nuclei were counterstained with DAPI. Antibody information is provided in Supplementary Table S3.

**Immunohistochemistry (IHC)**

Paraffin-embedded tissue sections (4 μm) were subjected to antigen retrieval in sodium citrate buffer. After blocking with 10% bovine serum albumin, sections were incubated overnight at 4 °C with primary antibodies against Ki-67, YBX1, DEPDC1, or β-catenin. Following incubation of sections with a secondary antibody, signals were developed with 3,3′-diaminobenzidine, and nuclei were counterstained with haematoxylin. After dehydration and mounting, protein expression was evaluated by light microscopy. All antibody information is provided in Supplementary Table S3.

**Animal experiments**

Female BALB/c nude mice (4–6 weeks old) were purchased from the Animal Center of Nanjing Medical University. Animal experiments adhered to institutional ethical guidelines.

For cell-derived xenograft models, nude mice were inoculated subcutaneously with SK-MES-1 cells stably transfected with one of four constructs (sh-NC, sh-

RP4-694A7.2, vector, or RP4-694A7.2). Tumor volume (calculated as $V$ = length × width² / 2) and body weight were monitored every 3 days. Mice were euthanized when tumors reached 15 mm in diameter, and tumors were collected for haematoxylin and eosin (H&E) and IHC staining.

For the PDX models, NSCLC patient tissue fragments were implanted subcutaneously. When tumor volumes reached 30–50 mm³, mice were randomized into three groups ($n$ = 5 per group): (a) blank control (5% glucose); (b) si-NC; (c) si-RP4-694A7.2. si-NC or si-RP4-694A7.2 (10 μg per tumor per dose) in 5% glucose was administered intratumorally using in vivo-jetPEI® (Polyplus, France) every 3 days for eight doses. Tumor growth and body weights were monitored as described above. At the endpoint, tumors were harvested for analysis.

## Bioinformatic and statistical analysis

Statistical analyses were performed using SPSS 19.0 and GraphPad Prism 8.0. Data are presented as mean ± standard deviation (SD). Differences between groups were evaluated using two-tailed Student's t-test or one-way analysis of variance. $P < 0.05$ was considered to indicate statistical significance. Bioinformatics databases are listed in Supplementary Table S4.

# Results

## RP4-694A7.2 is upregulated in NSCLC tissues and cells

In our previous study using NSCLC PDX models, we observed that third-generation xenograft tumors (X-3) grew more rapidly than primary tumors (X-1). Moreover, microarray analysis of lncRNA expression profiles revealed that these X-3 tumors were transcriptionally distinct from the primary tumors [10]. To explore the clinical roles and underlying mechanisms of these lncRNAs in NSCLC proliferation, we focused on the top 30 lncRNAs identified in PDX models and RNA sequencing (RNA-seq) data from The Cancer Genome Atlas (TCGA) NSCLC dataset (Fig. 1A; Supplementary Table S5, S6). Overlap analysis revealed that lncRNAs RP4-694A7.2 and RP11-106E15.1 were consistently identified in both datasets (Fig. 1B). To further confirm their expression in primary tumors and corresponding X-3 tumors, we performed RT-qPCR. Expression of RP4-694A7.2 was markedly upregulated in the X-3 group, whereas RP11-106E15.1 showed no differential expression (Fig. 1C; Supplementary Fig. S1A). Therefore, we selected RP4-694A7.2 for further investigation. Given that the role of RP4-694A7.2 had not been well characterized in NSCLC, we initially evaluated its expression in 20 paired tumor tissues and adjacent normal tissues (ANTs). RP4-694A7.2 expression was markedly higher in NSCLC tissues than in ANTs, as confirmed by RT–qPCR (Fig. 1D) and RNA-FISH with an RP4-694A7.2 probe (Fig. 1E). Similarly, its expression was elevated in NSCLC cell lines compared with BEAS-2B cells (Fig. 1F). Kaplan–Meier analysis of data from the GEPIA2 database further revealed that elevated RP4-694A7.2 expression predicted poorer overall survival in NSCLC patients (Fig. 1G). Moreover, knockdown of

RP4-694A7.2 in primary NSCLC cells established in our laboratory significantly reduced cell proliferation (Fig. 1H; Supplementary Fig. S1B–D).

RP4-694A7.2 is located on human chromosome 1 and consists of two exons with a total length of 960 nt according to the UCSC and Ensembl genome browser databases (Supplementary Fig. S1E,F). Its potential non-coding ability was analyzed using the ORFfinder and CPC2 databases (Supplementary Fig. S1G,H). Nuclear/cytoplasmic RNA fractionation assays revealed that RP4-694A7.2 was present in cytoplasm and nucleus of NSCLC cells (Fig. 1I; Supplementary Fig. S1I), as confirmed by RNA-FISH in NSCLC cells (Fig. 1J). In summary, RP4-694A7.2 is markedly upregulated in NSCLC tissues and cell lines, and its expression is correlated with cell proliferation.

**RP4-694A7.2 promotes NSCLC proliferation in vitro and in vivo**

To further investigate the role of RP4-694A7.2 in NSCLC proliferation, we knocked down or overexpressed RP4-694A7.2 in NSCLC cell lines (Fig. 2A,B; Supplementary Fig. S2A). RP4-694A7.2 knockdown reduced viability (by CCK-8 assay) and colony formation in SK-MES-1 and A549 cells. Conversely, overexpression of RP4-694A7.2 enhanced these characteristics of NCI-H520 cells (Fig. 2C–F; Supplementary Fig. S2B,C). Similarly, knockdown of RP4-694A7.2 decreased the percentage of EdU-positive SK-MES-1 and A549 cells, and overexpression increased it in NCI-H520 cells (Fig. 2G,H; Supplementary Fig. S2D). Flow cytometry analysis showed that RP4-694A7.2 knockdown

resulted in a lower proportion of cells in S phase and a higher proportion in G1 phase compared with controls, indicating that RP4-694A7.2 knockdown induced G1 arrest. Conversely, RP4-694A7.2 overexpression promoted G1/S transition (Fig. 2I,J; Supplementary Fig. S2E). Western blotting further revealed that RP4-694A7.2 silencing downregulated proliferation-related protein PCNA and G1/S transition promoters CDK4 and CDK6, whereas it upregulated cell cycle inhibitor $p27^{Kip1}$ (p27). RP4-694A7.2 overexpression had the opposite effects (Fig. 2K,L; Supplementary Fig. S2F). These results indicate that RP4-694A7.2 promotes NSCLC cell proliferation by accelerating G1/S transition.

To assess the impact of RP4-694A7.2 on tumor growth in vivo, we established cell-derived xenograft models in BALB/c nude mice with stable knockdown or overexpression of RP4-694A7.2 (Fig. 2M, N, R). Mice bearing RP4-694A7.2-knockdown tumors exhibited significantly lower tumor volumes and weights than controls, whereas those with RP4-694A7.2-overexpressing tumors showed the opposite effect (Fig. 2O, P, S, T). Consistently, Ki-67 IHC of xenograft sections confirmed that RP4-694A7.2 overexpression promoted tumor growth whereas its silencing inhibited tumor progression (Fig. 2Q,U). These findings indicate that RP4-694A7.2 promotes NSCLC growth both in vitro and in vivo.

**RP4-694A7.2 binds to YBX1 and inhibits its ubiquitin–proteasomal degradation**

The published literature shows that lncRNAs generally perform their biological

functions by interacting with RNA-binding proteins (RBPs) [11-13]. Therefore, we performed a biotin-labeled RNA pull-down assay followed by mass spectrometry (MS) to identify RP4-694A7.2-associated RBPs involved in NSCLC proliferation (Fig. 3A,B). Approximately 87 potential interacting proteins were pulled down with RP4-694A7.2 probe in NSCLC cells (Supplementary Table S7). We also used online tool catRAPID to predict RBPs of RP4-694A7.2. The most frequently detected RNA-binding motifs in the prediction results were then analyzed (Supplementary Fig. S3A). YBX1 was identified by both methods as the most likely binding partner of RP4-694A7.2 (Fig. 3C,D).

YBX1, a DNA/RNA-binding protein that causes dysregulation of multiple genes involved in cancer proliferation, metastasis, apoptosis and drug resistance [14-16], is upregulated in NSCLC and promotes NSCLC progression [17]. Correlation analysis of data from GEPIA2 showed that RP4-694A7.2 expression was positively associated with YBX1 expression in NSCLC (Supplementary Fig. S3B). We further validated the interaction between RP4-694A7.2 and YBX1 through RNA pull-down and RIP assays (Fig. 3E; Supplementary Fig. S3C) and predicted the secondary structure of RP4-694A7.2 using RNAfold software (Fig. 3F). To map the binding regions of RP4-694A7.2 to YBX1, we constructed one biotinylated full-length transcript and three biotinylated truncated fragments of RP4-694A7.2 for RIP assays using NSCLC cell lysates. Deletion-mapping analysis showed that nucleotides 238–559 of RP4-694A7.2 were indispensable for its interaction with YBX1 (Fig. 3G). YBX1 comprises three domains, an N-

353 terminal domain, a cold shock domain, and a large C-terminal domain (CTD). The
354 CTD contains a nuclear localization signal, cytoplasmic retention signal, and 20S
355 proteasome cleavage site [18]. To identify the domain involved in the binding of
356 YBX1 to RP4-694A7.2, we cloned a series of HA-tagged truncated YBX1 proteins
357 (Fig. 3H); an RNA pull-down assay showed that the interaction between RP4-
358 694A7.2 and YBX1 occurred through amino acids 130–219 in the CTD of YBX1
359 (Fig. 3I).

360 To further investigate the relationship between RP4-694A7.2 and YBX1, we
361 knocked down or overexpressed RP4-694A7.2 in NSCLC cells; silencing RP4-
362 694A7.2 markedly reduced protein levels of YBX1, whereas overexpression of
363 RP4-694A7.2 increased them, with neither manipulation affecting the mRNA
364 levels of YBX1 (Fig. 3J,K; Supplementary Fig. S3D–F), indicating that RP4-
365 694A7.2 regulates YBX1 levels via post-translational modification. Next, RP4-
366 694A7.2-knockdown and RP4-694A7.2-overexpressing cells were treated with
367 cycloheximide (CHX); western blot analysis showed that RP4-694A7.2
368 knockdown suppressed YBX1 protein stability under CHX treatment, whereas
369 RP4-694A7.2 overexpression prolonged its half-life (Fig. 3L,M), suggesting that
370 RP4-694A7.2 enhances YBX1 protein stability. To determine whether YBX1
371 degradation occurred via the proteasomal or lysosomal pathway, NSCLC cells
372 were treated with MG132 (a proteasome inhibitor) or Chloroquine (CQ, a
373 lysosome inhibitor). The destabilization of YBX1 by RP4-694A7.2 knockdown
374 was reversed by MG132 but not by CQ, and treatment with MG132 (but not CQ)

375 further increased YBX1 levels in RP4-694A7.2-overexpressing cells compared
376 with vector control cells (Fig. 3N,O; Supplementary Fig. S3G,H). Moreover,
377 polyubiquitination of YBX1 was markedly increased in RP4-694A7.2 knockdown
378 cells but decreased in RP4-694A7.2-overexpressing cells (Fig. 3P,Q). These
379 findings suggest that RP4-694A7.2 stabilizes the YBX1 protein by inhibiting its
380 ubiquitin–proteasome degradation (Fig. 3R).

381 Next, the role of the RP4-694A7.2/YBX1 regulatory axis in NSCLC proliferation
382 was characterized. CCK-8, colony formation, EdU, and western blot assays
383 showed that knockdown of YBX1 reduced the proliferative activity of A549 cells
384 compared with the control group (Supplementary Fig. S3I–N). In rescue
385 experiments, depletion of YBX1 abrogated the enhanced proliferation of RP4-
386 694A7.2-overexpressing NCI-H520 cells (Fig. 3S,T; Supplementary Fig. S3O,P).
387 Taken together, these findings indicate that RP4-694A7.2 promotes NSCLC cell
388 proliferation by directly interacting with YBX1.

389

390 **RP4-694A7.2 stabilizes YBX1 by suppressing WWP2-mediated**
391 **ubiquitination**

392 To further identify E3 ubiquitin ligases or deubiquitinases for YBX1, we combined
393 UbiBrowser-based prediction with MS analysis of YBX1 immunoprecipitates
394 (Supplementary Table S8, 9). Intersection of the two datasets yielded three
395 candidate E3 ubiquitin ligases: PRPF19, ITCH, and WWP2 (Fig. 4A). Notably,
396 WWP2 had the highest fold change as a YBX1-interacting protein in the MS

analysis (Supplementary Table S9), and GEPIA2 database analysis revealed that among the three candidate E3 ubiquitin ligases, only WWP2 showed a specific negative correlation with YBX1 (Fig. 4B; Supplementary Fig. S4A). Therefore, WWP2 was considered to be the E3 ligase most likely to interact with YBX1 and mediate its ubiquitin–proteasomal degradation in NSCLC. Co-IP analysis demonstrated endogenous and exogenous interactions between YBX1 and WWP2 (Fig. 4C,D; Supplementary Fig. S4B), and an IF staining assay confirmed their colocalization in the cytoplasm and nucleus of NSCLC cells (Fig. 4E). Moreover, molecular docking simulations using PyMOL software revealed a substantial interaction between YBX1 and WWP2, involving the formation of hydrogen bonds (Fig. 4F). We further found that overexpression of WWP2 reduced YBX1 protein levels in a dose-dependent manner, whereas WWP2 knockdown increased them (Fig. 4G; Supplementary Fig. S4C), with no effects on mRNA levels in either case (Supplementary Fig. S4D). The half-life of endogenous YBX1 was diminished in WWP2-overexpressing NSCLC cells but increased in WWP2-knockdown cells following CHX treatment (Fig. 4H; Supplementary Fig. S4E). Supplementation with MG132 markedly restored basal YBX1 levels in WWP2-overexpressing cells and further elevated YBX1 levels in WWP2-knockdown cells, confirming that WWP2 regulates YBX1 through proteasomal degradation (Fig. 4I; Supplementary Fig. S4F). WWP2 overexpression enhanced YBX1 ubiquitination, whereas WWP2 knockdown suppressed it (Fig. 4J; Supplementary Fig. S4G). Moreover, WWP2

overexpression facilitated K48-linked polyubiquitination but not K63-linked ubiquitination of YBX1 in NSCLC cells (Fig. 4K; Supplementary Fig. S4H).

Next, we examined whether RP4-694A7.2 affected the interaction between WWP2 and YBX1. Neither knockdown nor overexpression of RP4-694A7.2 altered WWP2 mRNA or protein levels in NSCLC cells (Supplementary Fig. S4I,J). However, WWP2 antibody co-immunoprecipitated more YBX1 from si-RP4-694A7.2-transfected cells than from si-NC controls, whereas less YBX1 was co-immunoprecipitated upon RP4-694A7.2 overexpression (Fig. 4L,M). Thus, these results indicate that RP4-694A7.2 stabilizes YBX1 by suppressing its WWP2-mediated ubiquitin–proteasomal degradation (Fig. 4N).

**RP4-694A7.2 promotes YBX1 nuclear import by enhancing the YBX1–KPNA2 interaction**

As a master regulator of cancer cell biology, YBX1 functions in the cytoplasm and nucleus [19]. YBX1 is localized predominantly in the cytoplasm under basal conditions but is translocated to the nucleus under specific intracellular or extracellular signals [20]. Therefore, we considered whether RP4-694A7.2 affected YBX1 nuclear import. Subcellular fractionation in NSCLC cells followed by western blotting showed that depletion of RP4-694A7.2 led to retention of YBX1 in the cytoplasm (Fig. 5A; Supplementary Fig. S5A), whereas RP4-694A7.2 overexpression increased the proportion of nuclear YBX1 (Fig. 5B). IF analysis of NSCLC cells confirmed these findings (Fig. 5C,D). Thus, RP4-

694A7.2 may contribute to YBX1 nuclear import in NSCLC cells.

We further investigated the mechanism of YBX1 nuclear import. KPNA2, a member of the alpha protein family of nuclear transporters, has been reported to interact with YBX1 and significantly facilitate its nuclear import in osteosarcoma [21, 22]. Their interaction was also identified in our MS analysis of YBX1 immunoprecipitates (Supplementary Table S9). Thus, we hypothesized that RP4-694A7.2 might promote YBX1 nuclear import via KPNA2. IF staining confirmed the colocalization of YBX1 and KPNA2 proteins in the cytoplasm and nucleus of NSCLC cells (Fig. 5E), and co-IP analysis further demonstrated their endogenous interactions (Fig. 5F; Supplementary Fig. S5B). RIP and RNA pull-down assays showed that RP4-694A7.2 could directly interact with KPNA2 in NSCLC cells (Fig. 5G,H; Supplementary Fig. S5C,D). Moreover, RP4-694A7.2 knockdown efficiently attenuated the interaction between YBX1 and KPNA2, whereas RP4-694A7.2 overexpression enhanced it (Fig. 5I,J). In summary, these findings indicate that RP4-694A7.2 promotes the nuclear import of YBX1 by enhancing the interaction between YBX1 and KPNA2 in NSCLC cells (Fig. 5K).

**RP4-694A7.2 promotes DEPDC1 transcription by strengthening YBX1 binding to the DEPDC1 promoter**

YBX1, a well-established transcription factor, binds to the promoters of certain genes in the nucleus to activate their transcription [23, 24]. To further elucidate the mechanism by which the RP4-694A7.2/YBX1 axis drives oncogenesis in

NSCLC, we performed RNA-seq in SK-MES-1 cells with or without RP4-694A7.2 knockdown. This analysis identified 88 upregulated and 367 downregulated genes ($P < 0.05$, |fold change| ≥ 1.5; Fig. 6A; Supplementary Table S10). The intersection of genes regulated by RP4-694A7.2 or YBX1 yielded five potential targets: IGFBP3, DEPDC1, HHIP, CYP24A1, and FOS (Fig. 6B; Supplementary Table S10–12). Notably, RT-qPCR analysis indicated that *DEPDC1* was consistently the most downregulated gene following knockdown of either RP4-694A7.2 or YBX1 in SK-MES-1 cells (Fig. 6C,D). GEPIA2 analysis also showed that DEPDC1 expression was positively correlated with that of RP4-694A7.2 and YBX1 in NSCLC (Fig. 6E). IF staining revealed that DEPDC1 was predominantly localized in the nucleus in NSCLC cells (Supplementary Fig. S6A). DEPDC1 is an oncogenic molecule with roles in cell mitosis, proliferation, and apoptosis in various cancers, including NSCLC [25, 26]. Hence, we focused on the role of DEPDC1 in RP4-694A7.2/YBX1-axis-dependent NSCLC proliferation.

Western blotting and RT-qPCR analyses showed that DEPDC1 mRNA and protein levels were markedly reduced following knockdown of either RP4-694A7.2 or YBX1 but were elevated upon their overexpression (Fig. 6C, D,F,G; Supplementary Fig. S6B–E). In rescue assays, YBX1 overexpression reversed the decrease in DEPDC1 levels caused by RP4-694A7.2 knockdown in SK-MES-1 cells, whereas in NCI-H520 cells, YBX1 knockdown attenuated the increase in DEPDC1 levels induced by RP4-694A7.2 overexpression (Fig. 6H). Although transcriptional regulation is a key mechanism by which DEPDC1 drives

485 the proliferation of NSCLC [27], how YBX1 regulates *DEPDC1* transcription
486 remains unclear. We therefore used JASPAR to predict YBX1 binding sites within
487 the *DEPDC1* promoter and identified two high-confidence response elements
488 (Fig. 6I; Supplementary Fig. S6F). Next, we constructed luciferase reporters
489 driven by the vector control, WT *DEPDC1* promoter, or mutant promoters (Mut1:
490 -TGTCCCATC-; Mut2: -TGTAACATC-) and co-transfected them with an HA-
491 YBX1 plasmid into HEK293T cells for luciferase reporter assays. Upon YBX1
492 overexpression, the WT and Mut1 *DEPDC1* reporters showed increased
493 luciferase activity compared with the vector control, whereas the Mut2 *DEPDC1*
494 reporter showed no significant change (Fig. 6J). These results confirmed that the
495 YBX1 binding site was located within the -TGTAACATC- sequence of the
496 *DEPDC1* promoter. To determine whether RP4-694A7.2 recruited YBX1 to
497 activate *DEPDC1* transcription, we detected the transcriptional activity of the
498 *DEPDC1* promoter after altering the expression of RP4-694A7.2. Luciferase
499 reporter assays showed that, upon YBX1 overexpression, RP4-694A7.2
500 knockdown in SK-MES-1 cells decreased the activity of the WT and Mut1
501 *DEPDC1* reporters, whereas RP4-694A7.2 overexpression in NCI-H520 cells
502 increased the activity of these reporters. However, the activity of the Mut2
503 *DEPDC1* reporter remained unchanged upon either knockdown or
504 overexpression of RP4-694A7.2 (Fig. 6K). ChIP analysis also demonstrated that
505 RP4-694A7.2 knockdown significantly reduced YBX1-mediated *DEPDC1*
506 transcriptional activation in SK-MES-1 cells, whereas its overexpression

enhanced YBX1 binding to the *DEPDC1* promoter in NCI-H520 cells (Fig. 6L). To investigate the role of DEPDC1 in RP4-694A7.2-mediated NSCLC proliferation, we knocked down DEPDC1 in NSCLC cells and confirmed the knockdown efficiency at mRNA and protein levels (Supplementary Fig. S6G,H). CCK-8, colony formation, EdU, and western blot assays showed that DEPDC1 knockdown reduced the proliferation of A549 cells compared with the control group (Supplementary Fig. S6I–L). Rescue assays further demonstrated that knockdown of DEPDC1 attenuated the pro-proliferative effect of RP4-694A7.2 overexpression in NCI-H520 cells (Fig. 6M,N; Supplementary Fig. S6M,N). Collectively, these findings reveal that the RP4-694A7.2/YBX1 axis promotes NSCLC proliferation by transcriptionally activating *DEPDC1* (Fig. 6O).

**RP4-694A7.2 promotes NSCLC proliferation by activating the Wnt/β-catenin pathway**

To understand the underlying biological pathways by which RP4-694A7.2 facilitated NSCLC proliferation, we analyzed RNA-seq data of SK-MES-1 cells transfected with si-RP4-694A7.2 or si-NC (Supplementary Table S10). Gene ontology (GO) enrichment analysis revealed that the differentially expressed genes were mainly involved in biological processes including cell proliferation, apoptosis, and the cell cycle (Fig. 7A,B). Kyoto Encyclopedia of Genes and Genomes (KEGG) pathway analysis and gene set enrichment analysis (GSEA) both showed marked enrichment of genes involved in the Wnt signaling pathway

(Fig. 7C,D). Therefore, we hypothesized that RP4-694A7.2 might play an important part in activation of the Wnt/β-catenin pathway in NSCLC. Western blot analysis showed that β-catenin and downstream proteins (cyclin D1 and c-Myc) were decreased by RP4-694A7.2 depletion but increased by its overexpression (Fig. 7E,F; Supplementary Fig. S7A). Subcellular fractionation of NSCLC cells followed by western blotting further revealed that RP4-694A7.2 knockdown reduced nuclear β-catenin protein levels, whereas its overexpression increased them (Fig. 7G,H; Supplementary Fig. S7B). Consistently, TOP/FOP Flash assays in NSCLC cells showed that RP4-694A7.2 silencing suppressed β-catenin-dependent reporter activity, whereas its overexpression significantly increased luciferase activity (Fig. 7I,J). These results indicate that RP4-694A7.2 activates the Wnt/β-catenin signaling pathway in NSCLC cells.

To further investigate whether RP4-694A7.2 promoted NSCLC proliferation via the Wnt/β-catenin pathway, we first confirmed that knockdown of β-catenin or treatment with Wnt pathway inhibitor IWR-1 markedly reduced protein levels of β-catenin, cyclin D1, and c-Myc (Supplementary Fig. S7C). Next, CCK-8, colony formation, EdU, and western blot assays showed that β-catenin knockdown significantly inhibited the proliferation of A549 cells (Supplementary Fig. S7D–F). Rescue assays further confirmed that β-catenin knockdown effectively counteracted the pro-proliferative effect of RP4-694A7.2 overexpression in NCI-H520 cells (Fig. 7K,L; Supplementary Fig. S7G,H). Previous studies have reported that YBX1 and DEPDC1 proteins can regulate the malignant

progression of tumors through the Wnt/β-catenin pathway [28-31]. Here, we found that knockdown of either YBX1 or DEPDC1 attenuated the Wnt/β-catenin pathway activation induced by RP4-694A7.2 overexpression (Supplementary Fig. S7I,J). Moreover, we performed IHC staining on the xenograft tissues shown in Fig. 2P and 2T. Overexpression of RP4-694A7.2 increased the protein levels of YBX1, DEPDC1, and β-catenin, whereas knockdown of RP4-694A7.2 decreased them (Fig. 7M; Supplementary Fig. S7K). Similarly, protein levels of YBX1, DEPDC1, and β-catenin were higher in NSCLC tissues than in ANTs (Fig. 7N). Together, these results demonstrate that the RP4-694A7.2/YBX1/DEPDC1 axis promotes NSCLC proliferation by activating the Wnt/β-catenin pathway.

**RP4-694A7.2 is a potential therapeutic target for NSCLC**

To assess the therapeutic potential of targeting RP4-694A7.2 in NSCLC, we knocked down its expression in patient-derived primary NSCLC cells. Colony formation, CCK-8, and EdU assays demonstrated that RP4-694A7.2 knockdown markedly reduced the proliferation of these cells (Fig. 1H; Supplementary Fig. S1B–D), and flow cytometry revealed an increased proportion of cells in G1 phase, indicating arrest at this stage (Supplementary Fig. S8A). Consistently, RP4-694A7.2 knockdown decreased protein levels of CDK4, CDK6, and PCNA while increasing those of p27 (Supplementary Fig. S8B), as well as reducing protein levels of YBX1, DEPDC1, β-catenin, c-Myc, and cyclin D1 (Supplementary Fig. S8C,D). These results indicate that the RP4-

694A7.2/YBX1/DEPDC1/Wnt/β-catenin regulatory axis plays a critical part in proliferation of primary NSCLC cells.

Given the utility of PDX models for the evaluation of in vivo therapeutic efficacy [32], we established such models in nude mice using tumor specimens from the same patient who provided the primary NSCLC cells. Tumor-bearing mice were randomly allocated into three groups for intratumoral injection: blank control (glucose solution), si-NC, and si-RP4-694A7.2. The si-NC and si-RP4-694A7.2 groups were established using in vivo-jetPEI, which enables efficient nucleic acid delivery to tumor cells [33, 34] (Fig. 8A). RP4-694A7.2 knockdown inhibited tumor growth compared with the blank control and si-NC groups (Fig. 8B), and tumors in the si-RP4-694A7.2 group exhibited reduced tumor size and weight at the endpoint (day 21 post-injection) (Fig. 8C,D). Moreover, RT-qPCR analysis confirmed that RP4-694A7.2 expression was significantly downregulated in the si-RP4-694A7.2 group (Fig. 8E). To evaluate the systemic toxicity of the therapy, we monitored mouse body weight and observed no significant differences between groups, indicating that treatment was well tolerated (Fig. 8F). IHC staining revealed that the protein levels of Ki67, YBX1, DEPDC1, and β-catenin were markedly lower in the si-RP4-694A7.2 group than in the blank control or si-NC groups (Fig. 8G). Collectively, these findings demonstrate that knockdown of RP4-694A7.2 markedly suppresses NSCLC primary cell proliferation and tumor growth, highlighting RP4-694A7.2 as a promising therapeutic target for this malignancy.

## Discussion

Aberrant lncRNA expression is a molecular hallmark of cancer and contributes to multiple oncogenic processes, including proliferation, motility, replicative immortality, angiogenesis, and cell survival, particularly in NSCLC [35, 36]. In this study, we found that lncRNA RP4-694A7.2 was markedly upregulated in NSCLC tissues and cells. Functional studies revealed that RP4-694A7.2 promoted NSCLC proliferation by accelerating the G1/S phase transition. Mechanistically, RP4-694A7.2 directly bound to YBX1 and suppressed its WWP2-mediated ubiquitination, thereby blocking proteasomal degradation and enhancing YBX1 stability. Furthermore, RP4-694A7.2 strengthened the YBX1–KPNA2 interaction to facilitate YBX1 nuclear import. Nuclear-accumulated YBX1 subsequently bound to the *DEPDC1* promoter to activate its transcription, which in turn stimulated the Wnt/β-catenin signaling pathway. Collectively, our findings identify a critical RP4-694A7.2/YBX1/DEPDC1/Wnt/β-catenin regulatory axis and highlight RP4-694A7.2 as a potential therapeutic target for NSCLC.

Accumulating evidence shows that the proteasome pathway is pivotal in regulation of YBX1 stability, and lncRNAs have been reported to modulate this process through ubiquitin-dependent mechanisms [37, 38]. Here, we demonstrated that nucleotides 238–559 of RP4-694A7.2 directly bound to the CTD (amino acids 130–219) of YBX1, suppressing WWP2-mediated K48-linked ubiquitination and then inhibiting proteasomal degradation of YBX1, thereby strengthening YBX1 stability. WWP2 is an E3 ubiquitin ligase belonging to the

NEDD4-like protein family and is involved in the regulation of membrane protein trafficking, protein degradation, transcription, and apoptosis [39, 40]. This study identified YBX1 as a novel target protein of WWP2 and demonstrated the existence of an important mechanism involving the RP4-694A7.2/WWP2/YBX1 axis. Furthermore, recent studies have shown that in hepatocellular carcinoma, circZNF79 protects YBX1 from autophagy–lysosome degradation by removing the K63 ubiquitin chain, without affecting proteasomal degradation [41]. By contrast, we found that in NSCLC, RP4-694A7.2 protected YBX1 from proteasomal degradation by inhibiting K48-linked ubiquitination, without affecting lysosomal degradation. This difference highlights the complexity and tumor specificity of the mechanisms regulating YBX1 stability, providing a rationale for either combination therapy or subtype-specific therapy targeting YBX1 in clinical practice.

The formation of the RP4-694A7.2/KPNA2/YBX1 complex has a key role in regulation of the subcellular localization and transcriptional activity of YBX1 in NSCLC. Our mechanistic analysis indicated that KPNA2, a nuclear import receptor, interacted with YBX1 and mediates its transport from the cytoplasm to the nucleus, thereby enhancing the nuclear accumulation of YBX1 in NSCLC cells; this was consistent with previous reports in osteosarcoma [21]. Although we found that RP4-694A7.2 markedly promoted YBX1 nuclear import by enhancing its interaction with KPNA2, the detailed mechanism remained unclear. Published studies have shown that KPNA2 promotes phosphorylation and

nuclear import of STAT3 by facilitating the binding of STAT3 to the phosphorylated kinase JAK1 [42]. Therefore, future studies will investigate the possibility of KPNA2-mediated YBX1 phosphorylation in NSCLC and assess the role of RP4-694A7.2 expression in this mechanism. We further demonstrated that nuclear-accumulated YBX1 binds to a specific motif (-TGTAACATC-) in the *DEPDC1* promoter, promoting *DEPDC1* transcription and subsequently activating the Wnt/β-catenin pathway. Although YBX1 is recognized as a broad regulator of transcription, its recruitment to the *DEPDC1* promoter by a lncRNA has not previously been reported. Consequently, this work identifies the RP4-694A7.2/YBX1/DEPDC1 axis as a novel regulatory cascade in NSCLC. Moreover, given the well-established roles of Wnt/β-catenin signaling in NSCLC stemness [43], metastasis [44], and therapy resistance [45], this axis may be involved in various oncogenic processes, making it a potential therapeutic target for combination therapy.

From a translational perspective, the most important aspect of our study is the closed-loop pipeline for RP4-694A7.2, in which we identified the target using PDX models, elucidated its underlying mechanism in NSCLC tissues and cells, and validated its therapeutic efficacy in PDX models. Intratumoral administration of RP4-694A7.2-targeting siRNA complexed with in vivo-jetPEI markedly suppressed tumor growth and reduced expression of YBX1, DEPDC1 and β-catenin in NSCLC PDX models without evident systemic toxicity, demonstrating the therapeutic efficacy and safety of this approach. Notably, PDX models retain

661 the heterogeneity and stromal architecture of the original patient tumors; thus,
662 our results provide preclinical evidence supporting the feasibility and translational
663 potential of RP4-694A7.2-targeted therapy. The design of effective siRNA-based
664 therapeutics against lncRNAs specifically exploits the structural features of the
665 lncRNAs, which include flexible secondary structures rich in single-stranded
666 regions and stem–loop bulges. These structures provide ample binding interfaces
667 for nucleic acid therapeutics such as antisense oligonucleotides and siRNAs.
668 Consistent with this, we identified two effective siRNAs targeting the predicted
669 stem-loop region in the RP4-694A7.2 secondary structure. Recent advances in
670 RNA three-dimensional structural data have further delineated precise interaction
671 interfaces and targetable regions between lncRNAs and proteins, peptides, DNA
672 and other RNAs, indicating new approaches to disrupting lncRNA–
673 biomacromolecule interactions or guiding antisense oligonucleotide design [46].
674 Delivery of siRNA can be broadly categorized into localized and systemic delivery.
675 Localized delivery provides optimal bioavailability at the intended site and
676 circumvents the obstacles associated with systemic administration. Organs such
677 as the eyes, mucous membranes and skin, as well as local tumors, are suitable
678 for localized delivery; this includes intranasal and intratracheal delivery targeting
679 lung diseases, which have shown better responses and increased bioavailability
680 of the drug compared with other approaches [47]. For NSCLC, intratracheal
681 delivery of RP4-694A7.2-targeting siRNA may represent a feasible route for
682 clinical translation. Collectively, these findings support the use of RP4-694A7.2-

targeting siRNAs as a promising therapeutic strategy for NSCLC.

Our study had several limitations. First, its limited clinical sample size may restrict the statistical power and generalizability of our conclusions. Consequently, multi-center prospective studies with larger cohorts, including individuals with various NSCLC subtypes, will be required to confirm the correlation between RP4-694A7.2 expression and tumor proliferative activity and to evaluate its prognostic significance in NSCLC patients. Second, this study primarily focused on the proliferative activity of NSCLC and did not investigate the relationship of RP4-694A7.2 with cell migration, invasion, or drug resistance. Future studies should validate these aspects using transwell migration assays, half-maximal inhibitory concentration assays, and flow-cytometry-based apoptosis assays. Finally, although RP4-694A7.2 was shown to directly interact with KPNA2 in NSCLC cells, the specific nucleotide segment of RP4-694A7.2 and the amino acid domain of KPNA2 responsible for this interaction remain unknown. Truncated mutant plasmids of RP4-694A7.2 and KPNA2 could be used with RNA pull-down and RIP assays to elucidate these mechanisms.

## Conclusions

Our study identifies RP4-694A7.2 as a crucial oncogenic lncRNA in NSCLC. RP4-694A7.2 promotes NSCLC proliferation in cellular and animal models. Mechanistically, RP4-694A7.2 directly binds to YBX1, stabilizing it by blocking WWP2-mediated K48-linked ubiquitination and proteasomal degradation.

Moreover, RP4-694A7.2 facilitates YBX1 nuclear import by enhancing its interaction with KPNA2. The accumulated nuclear YBX1 subsequently binds to the DEPDC1 promoter to activate its transcription, thereby activating the Wnt/β-catenin signaling pathway and driving G1/S phase progression (Fig. 8H). These findings uncover a crucial RP4-694A7.2/YBX1/DEPDC1/Wnt/β-catenin regulatory axis driving NSCLC proliferation. Notably, this study also establishes a closed-loop PDX-to-mechanism-to-PDX translational pipeline, highlighting RP4-694A7.2 as a promising therapeutic target for NSCLC.

**Abbreviations**

| | |
|---|---|
| NSCLC | Non-small cell lung cancer |
| LncRNAs | Long noncoding RNAs |
| PDX | Patient-derived xenograft |
| YBX1 | Y-box binding protein 1 |
| WWP2 | WW domain-containing E3 ubiquitin protein ligase 2 |
| KPNA2 | Karyopherin subunit alpha 2 |
| DEPDC1 | DEP domain-containing 1 |
| MS | Mass spectrometry |
| FISH | Fluorescence in situ hybridization |
| IP | Immunoprecipitation |
| RIP | RNA immunoprecipitation |
| Co-IP | Co-immunoprecipitation |

| | |
|---|---|
| ChIP | Chromatin immunoprecipitation |
| IF | Immunofluorescence |
| IB | Immunoblotting |
| IHC | Immunohistochemistry |
| CQ | Chloroquine |
| WT | Wild-type |

## Declarations

### Ethics approval and consent to participate

All animal experiments were approved by the Ethics Committee of the First Affiliated Hospital of the University of Science and Technology of China on April 8, 2026 (Approval No. 2026-N(A)-068). All human tissues were anonymized and de-identified prior to inclusion in the study, and the use of these tissues was approved by the Ethics Committee of Anhui Provincial Hospital on June 21, 2016 (Approval No. 2016 Ethics Review No. 53).

### Data availability

All data generated or analysed during this study are included in this article and its supplementary information files. Additional data are available from the corresponding author upon reasonable request.

### Funding

This study was supported by the National Natural Science Foundation of China (81972006) and the Fundamental Research Funds for the Central Universities

(WK9110000101).

## Author contributions

DL conceived, designed, and wrote the manuscript. JL collected and assembled the data. WD performed the bioinformatics analysis. SZ carried out cell culture and collected NSCLC tissue samples. BH, MZ, and SY contributed to both in vivo and in vitro experiments. PL and BW were responsible for the accuracy and completeness of the study. All authors have read and approved the final manuscript.

## Consent for publication

Not applicable.

## Acknowledgements

Not applicable.

## Competing interests

The authors declare that they have no competing interests.

## References

1. Herbst RS, Morgensztern D, Boshoff C. The biology and management of non-small cell lung cancer. Nature. 2018;553(7689):446–54.
2. Kumar V, Yadavilli S, Kannan R. A review on RNAi therapy for NSCLC: Opportunities and challenges. Wiley Interdiscip Rev Nanomed Nanobiotechnol. 2021;13(2):e1677.
3. Herman AB, Tsitsipatis D, Gorospe M. Integrated lncRNA function upon genomic and epigenomic regulation. Mol Cell. 2022;82(12):2252–66.
4. Grillone K, Carida G, Luciano F, Cordua A, Di Martino MT, Tagliaferri P, et al. A systematic review of non-coding RNA therapeutics in early clinical trials: a new perspective against cancer. J Transl Med. 2024;22(1):731.
5. Huang L, Liu C, Zhao Z, Xie S, Sun Z, Liao X, et al. LncRNA SNHG8 promotes myocardial fibrosis by binding to E2F1 to induce MAD2L1 transcription. Int J Biol Macromol. 2025;331(Pt 1):148362.
6. Luo P, Lu D, Zhang S, Dong W, Fang K, Yu S, et al. A novel antisense lncRNA, LPCRL, functions

as a molecular scaffold for the USP15/MIB1 complex to promote primary cisplatin resistance and tumor progression in lung squamous cell carcinoma. J Exp Clin Cancer Res. 2026;45(1).
7. Tabbo F, Guerrera F, van den Berg A, Gaudiano M, Maletta F, Bessone L, et al. Kinomic profiling of tumour xenografts derived from patients with non-small cell lung cancer confirms their fidelity and reveals potentially actionable pathways. Eur J Cancer. 2021;144:17–30.
8. Yuan Y, Gao H, Li Y, Jiao X. The latest progress of personalized drug screening and therapy research for common clinical tumors through the PDX model platform. J Pharm Anal. 2025;15(10):101225.
9. Meehan TF. Know Thy PDX Model. Cancer Res. 2019;79(17):4324–5.
10. Lu D, Luo P, Zhang J, Ye Y, Wang Q, Li M, et al. Patient-derived tumor xenografts of lung squamous cell carcinoma alter long non-coding RNA profile but not responsiveness to cisplatin. Oncol Lett. 2018;15(6):8589–603.
11. Mahajan A, Chandran S, Kumar A, Chen L, Dhillon NK. LncRNA-536 and RNA-Binding Protein RBM25 Interactions in Pulmonary Artery Smooth Muscle Cells: Implications in Pulmonary Hypertension. Arterioscler Thromb Vasc Biol. 2025;45(8):e374–e91.
12. Rigaud VOC, Hoy RC, Kurian J, Zarka C, Behanan M, Brosious I, et al. RNA-Binding Protein LIN28a Regulates New Myocyte Formation in the Heart Through Long Noncoding RNA-H19. Circulation. 2023;147(4):324–37.
13. Parakkunnel R, Naik Keshava B, Sannagoudar MS, Jeevan Kumar SP, Jayaswall K, Sundaram A, et al. Integrative Analysis of lncRNA-RBP (RNA-Binding Protein) Regulatory Networks Reveals Molecular Targets for Enhancing Zea mays Resistance to Aspergillus flavus and Aflatoxin Contamination. Int J Mol Sci. 2026;27(5).
14. Qin S, Liu Y, Zhang X, Huang P, Xia L, Leng W, et al. lncRNA FGD5-AS1 is required for gastric cancer proliferation by inhibiting cell senescence and ROS production via stabilizing YBX1. J Exp Clin Cancer Res. 2024;43(1):188.
15. Hussain SA, Venkatesh T. YBX1/lncRNA SBF2-AS1 interaction regulates proliferation and tamoxifen sensitivity via PI3K/AKT/MTOR signaling in breast cancer cells. Mol Biol Rep. 2023;50(4):3413–28.
16. Hou Z, Cao C, Xiang M, Li G, Ma J, Zhang Y, et al. Celecoxib inhibits COX-2 and initiates YAP-dependent mitochondrial apoptosis via YBX1 shuttling in hepatocellular carcinoma. Cell Commun Signal. 2026;24(1).
17. Su H, Fan G, Huang J, Qiu X. LncRNA HOXC-AS3 promotes non-small-cell lung cancer growth and metastasis through upregulation of YBX1. Cell Death Dis. 2022;13(4):307.
18. Lyabin DN, Eliseeva IA, Ovchinnikov LP. YB-1 protein: functions and regulation. Wiley Interdiscip Rev RNA. 2014;5(1):95–110.
19. Goodarzi H, Liu X, Nguyen HC, Zhang S, Fish L, Tavazoie SF. Endogenous tRNA-Derived Fragments Suppress Breast Cancer Progression via YBX1 Displacement. Cell. 2015;161(4):790–802.
20. Eliseeva IA, Kim ER, Guryanov SG, Ovchinnikov LP, Lyabin DN. Y-box-binding protein 1 (YB-1) and its functions. Biochemistry (Mosc). 2011;76(13):1402–33.
21. Cao L, Jia K, Van Tine BA, Yu Y, Peng Y, Chen X, et al. KPNA2 promotes osteosarcoma progression by regulating the alternative splicing of DDX3X mediated by YBX1. Oncogene. 2025;44(26):2186–200.
22. Liu HT, Gao ZX, Li F, Guo XY, Li CL, Zhang H, et al. LncRNA LY6E-DT and its encoded metastatic-

related protein play oncogenic roles via different pathways and promote breast cancer progression. Cell Death Differ. 2024;31(2):188–202.
23. Leitz A, Kav B, Liu X, Fatafta H, Jankowski V, Aggeler B, et al. Guanidinylation of the cold shock protein YB-1: Molecular basis, structural changes and Notch-3 receptor binding. Protein Sci. 2025;34(7):e70188.
24. Duan Y, Li P, Yang Y, Wu G, Xing H, Chen H, et al. EPS8L2 drives colorectal cancer cell proliferation and migration via YBX1-dependent activation of G3BP2 transcription. Cell Death Dis. 2025;16(1):605.
25. Yan Y, Fu J. The human 18S rRNA m6A methyltransferase METTL5 promotes tumorigenesis via DEPDC1 in lung squamous cell carcinoma. Front Oncol. 2025;15:1522157.
26. Lv M, Li X, Yin Z, Yang H, Zhou B. Comprehensive analysis and validation reveal DEPDC1 as a potential diagnostic biomarker associated with tumor immunity in non-small-cell lung cancer. PLoS One. 2024;19(4):e0294227.
27. Lv M, Li X, Zheng C, Tian W, Yang H, Yin Z, et al. Exosomal miR-130b-3p suppresses metastasis of non-small cell lung cancer cells by targeting DEPDC1 via TGF-beta signaling pathway. Int J Biol Macromol. 2024;275(Pt 1):133594.
28. Zhu Q, Xu G, Wang T, Ding Z, Liu L, Ling L, et al. Downregulation of LRRC59 suppresses cervical cancer progression likely by inhibiting YBX1-mediated Wnt/beta-catenin signaling. Sci Rep. 2026;16(1).
29. Xi YH, Li CS, Wu PL, Zhou XY, Li QW, Shen CH. Y-Box-Binding Protein 1 Facilitates the Proliferation and Osteogenic Differentiation of Periodontal Ligament Stem Cells Through the Transcriptional Activation of FGF2-Mediated Akt/GSK3beta/beta-Catenin Signaling. Kaohsiung J Med Sci. 2025;41(12):e70079.
30. Huang G, Chen S, Washio J, Paka Lubamba G, Takahashi N, Li C. Glycolysis-Related Gene Analyses Indicate That DEPDC1 Promotes the Malignant Progression of Oral Squamous Cell Carcinoma via the WNT/beta-Catenin Signaling Pathway. Int J Mol Sci. 2023;24(3).
31. Geng G, Li Q, Guo X, Ni Q, Xu Y, Ma Z, et al. FOXO3a-modulated DEPDC1 promotes malignant progression of nephroblastoma via the Wnt/beta-catenin signaling pathway. Mol Med Rep. 2022;26(2).
32. Hare JI, Lammers T, Ashford MB, Puri S, Storm G, Barry ST. Challenges and strategies in anti-cancer nanomedicine development: An industry perspective. Adv Drug Deliv Rev. 2017;108:25–38.
33. Alhozeel B, Pandey SK, Shteinfer-Kuzmine A, Santhanam M, Shoshan-Barmatz V. Silencing the Mitochondrial Gatekeeper VDAC1 as a Potential Treatment for Bladder Cancer. Cells. 2024;13(7).
34. Huang Y, Zhu L, Wang J, Pan L, Yang Y, Li D. A miRNA cocktail orchestrates coordinated cellular responses to promote diabetic wound healing. Burns Trauma. 2025;13:tkaf060.
35. Gutschner T, Richtig G, Haemmerle M, Pichler M. From biomarkers to therapeutic targets-the promises and perils of long non-coding RNAs in cancer. Cancer Metastasis Rev. 2018;37(1):83–105.
36. Lin H, Li J, Wang M, Zhang X, Zhu T. Exosomal Long Noncoding RNAs in NSCLC: Dysfunctions and Clinical Potential. J Cancer. 2023;14(10):1736–50.
37. Wang X, Li X, Sun R, Zhang S, Jiao T, Lyu X, et al. LINC01116 promotes glycolysis by up-regulating HIF-1alpha via YBX1-mediated dual mechanism in lung cancer. Free Radic Biol Med. 2026;248:320–32.

38. Huo X, Zhang R, Shen Y, Zhang Q, Nan Y, Dong Y, et al. Linc00347 suppresses ferroptosis in drug-resistant gastric cancer cells through stabilizing FoxO6 mRNA mediated by YBX1. Int J Biol Macromol. 2026:152601.
39. Chen W, Jiang X, Luo Z. WWP2: a multifunctional ubiquitin ligase gene. Pathol Oncol Res. 2014;20(4):799–803.
40. Wang W, Wu W, Hao M, Cui S, Zhao S, Pei JF, et al. WWP2 underlies ROS-induced granulosa cell apoptosis by promoting ubiquitination of BAK in polycystic ovary syndrome. Cell Death Dis. 2026;17(1).
41. Guo X, Xi L, Liu Y, Lv W, Li T, Ju A, et al. Dysregulation of CircZNF79(5) Modulates YBX1 Stability and Selective Autophagy to Drive Hepatocellular Carcinoma Progression. Adv Sci (Weinh). 2026;13(6):e10310.
42. Jia Y, Wang Q, Liang M, Huang K. KPNA2 promotes angiogenesis by regulating STAT3 phosphorylation. J Transl Med. 2022;20(1):627.
43. Li KC, Gan S, Lu S, Yuan TK, Dong ZN, Gao C, et al. USP48 stabilizes YBX1 to enforce a Wnt-driven stemness circuit and osimertinib resistance in EGFR-mutant NSCLC. Cancer Lett. 2026:218587.
44. Wu JQ, Zou HP, Fan RY, Cai J, Wei P, He MF, et al. GNA13 promotes brain metastasis of non-small cell lung cancer and EMT through the WNT/beta catenin signaling pathway. Front Cell Dev Biol. 2025;13:1652200.
45. Zheng J, Lu Y, Yang M, Han Y, Wang E, Zhao H. DACT3-DVL1 Interaction-Mediated Canonical WNT Signaling Regulates Non-Small Cell Lung Cancer Progression and Cisplatin Resistance. FASEB J. 2025;39(16):e70975.
46. De Souza Degenhardt MF, Wang YX. Challenges and opportunities in technologies and methods for lncRNA structure determination. Cell Biosci. 2025;15(1):132.
47. Singh J, Saeedan AS, Kaithwas G, Ansari MN. Small interfering RNA: From designing to therapeutic in cancer. J Genet Eng Biotechnol. 2025;23(2):100484.

## Figure legends

**Fig. 1.** RP4-694A7.2 is upregulated in NSCLC tissues and cell lines. **(A)** Volcano plot of RNA-seq results showing lncRNAs differentially expressed between NSCLC tissues and normal samples from TCGA. **(B)** Venn diagram showing the overlap of genes from TCGA NSCLC RNA-seq data and the 30 top-ranked lncRNAs from previous NSCLC PDX models. **(C)** RP4-694A7.2 levels detected by RT-qPCR in primary tumors (X-1) and corresponding third-generation xenograft tumors (X-3). *n* = 6. **(D)** RP4-694A7.2 levels detected by RT-qPCR in

20 paired NSCLC tumor tissues and adjacent non-tumor tissues (ANTs). **(E)** Representative images of H&E staining and RP4-694A7.2 RNA-FISH staining of NSCLC tissues and ANTs. Scale bar: 100 μm. **(F)** RP4-694A7.2 levels detected by RT-qPCR in different NSCLC cell lines compared with BEAS-2B cells. **(G)** Kaplan–Meier analysis of overall survival rate in NSCLC patients according to RP4-694A7.2 expression in the GEPIA2 database. **(H)** Colony formation assay assessing proliferation of primary cells following RP4-694A7.2 knockdown. **(I)** Subcellular distribution of RP4-694A7.2 determined by RT-qPCR in SK-MES-1 and NCI-H520 cells; the nuclear and cytoplasmic controls were U6 and GAPDH, respectively. **(J)** RNA-FISH showing cytoplasmic and nuclear localization of RP4-694A7.2 in NSCLC cells. Nuclei were counterstained with DAPI (blue), and the RP4-694A7.2 probe was labeled with Cy3 (red). Scale bar: 100 μm. Data are presented as the mean ± SD from three independent experiments, with significance determined by Student's *t*-test (***P* < 0.01, ****P* < 0.001).

**Fig. 2.** RP4-694A7.2 promotes NSCLC growth both in vitro and in vivo. **(A)** Validation of RP4-694A7.2 expression in SK-MES-1 cells transfected with siRNAs. **(B)** Validation of RP4-694A7.2 expression in NCI-H520 cells transfected with overexpression plasmids. **(C–H)** CCK-8, colony formation, and EdU assays assessing the proliferation of NSCLC cells following RP4-694A7.2 knockdown or overexpression. Scale bar: 200 μm. **(I,J)** Cell cycle analysis by flow cytometry of PI-stained NSCLC cells. **(K,L)** Western blot analysis of PCNA, CDK4, CDK6, and

p27 levels in NSCLC cells with RP4-694A7.2 knockdown or overexpression. **(M)** Schematic of the subcutaneous implantation tumor model. **(N,R)** Validation of RP4-694A7.2 knockdown or overexpression efficiency in pLV-Neo-CMV-EGFP-based plasmids by RT-qPCR. **(O,S)** Tumor volumes were measured every 3 days, followed by tumor harvest on day 29. **(P,T)** Representative images and tumor weights from subcutaneous xenograft tumors. **(P)** sh-NC vs. sh-RP4-694A7.2 groups. **(T)** Vector vs. RP4-694A7.2 groups. **(Q,U)** Representative images of H&E staining and Ki-67 IHC in different groups of xenograft tumor tissues. Scale bars: 50 μm. Data are presented as the mean ± SD from three independent experiments, with significance determined by Student's *t*-test (***P* < 0.01, ****P* < 0.001).

**Fig. 3.** RP4-694A7.2 binds to YBX1 and decreases its ubiquitination. **(A)** Schematic workflow of the biotinylated RNA pull-down assay used to identify RP4-694A7.2-binding proteins. **(B)** Silver-stained sodium dodecyl sulfate polyacrylamide gel showing proteins pulled down from SK-MES-1 cell lysates by biotin-labeled RP4-694A7.2 in an RNA pull-down assay. **(C)** Venn diagram showing RBPs in the intersection of those identified by MS data and those predicted using the catRAPID database. **(D)** Representative YBX1 peptides binding to RP4-694A7.2 as detected by MS. **(E)** Specific association between RP4-694A7.2 and YBX1 in NSCLC cells validated by RNA pull-down and RIP assays. **(F)** Secondary structure of RP4-694A7.2 as predicted by RNAfold. The

944 inset (framed in red) shows the YBX1-binding stem–loop structures in RP4-
945 694A7.2. **(G)** RT-qPCR analysis of RP4-694A7.2 and its deletion mutants pulled
946 down in RIP assays with the anti-YBX1 antibody or IgG in SK-MES-1 cells. **(H)**
947 Schematic representation of YBX1 mutants, with mutations generated at the
948 indicated amino acid positions. **(I)** IB detection of HA-tagged YBX1 (WT versus
949 domain truncation mutants) precipitated by in vitro-transcribed biotinylated RP4-
950 694A7.2 in SK-MES-1 cells. **(J,K)** YBX1 protein levels assessed by western
951 blotting in NSCLC cells following RP4-694A7.2 knockdown or overexpression.
952 **(L,M)** Protein levels of YBX1 in NSCLC cells with RP4-694A7.2 knockdown or
953 overexpression under CHX (50 μg/mL) treatment for the indicated times,
954 determined by western blotting. Quantitative statistics for YBX1 protein levels are
955 shown on the right. **(N,O)** Protein levels of YBX1 in NSCLC cells with RP4-
956 694A7.2 knockdown or overexpression, treated with MG132 (20 μM, 5 h),
957 determined by western blotting. **(P,Q)** Effects of RP4-694A7.2 knockdown or
958 overexpression on YBX1 ubiquitination in NSCLC cells. IB was performed with
959 anti-ubiquitin (Ub) after cell lysates had been subjected to IP with anti-YBX1
960 beads. Cells were treated with MG132 (20 μM, 5 h) before being harvested. **(R)**
961 Model for RP4-694A7.2-mediated YBX1 stability. **(S,T)** CCK-8 and colony
962 formation assays assessing the proliferation of RP4-694A7.2-overexpressing
963 NCI-H520 cells following YBX1 knockdown. Data are presented as the mean ±
964 SD from three independent experiments, with significance determined by
965 Student's *t*-test (***P* < 0.01, ****P* < 0.001).

**Fig. 4.** RP4-694A7.2 enhances YBX1 protein stability by suppressing WWP2-mediated ubiquitination and proteasomal degradation of YBX1. **(A)** Simplified flow chart outlining the systematic screening process used to identify ubiquitin-protein ligases interacting with YBX1. IP-MS Immunoprecipitation-mass spectrometry. **(B)** Correlation between YBX1 and WWP2 expression in NSCLC according to GEPIA2 analysis. **(C,D)** Interaction between YBX1 and WWP2 assessed by co-IP assay in NSCLC cells, under both endogenous conditions and with exogenous overexpression. **(E)** Colocalization analysis of YBX1 and WWP2 in NSCLC cells by IF assay; scale bar: 20 μm. **(F)** Molecular docking analysis (PyMOL) suggesting a potential interaction between YBX1 and WWP2 (docking score: −369.69; confidence score: 0.9878). Red dashed lines indicate hydrogen bonding. **(G)** Protein level of HA-YBX1 in NSCLC cells transfected with gradually increasing numbers of Flag-WWP2 plasmids, determined by western blotting. **(H)** NSCLC cells transfected with Flag-WWP2 were treated with CHX (50 μg/mL) and harvested at the indicated time points for western blotting. The right panel shows quantitative analysis of YBX1 protein levels. **(I)** NSCLC cells transfected with Flag-WWP2 were treated with MG132 (20 μM, 5 h) before harvest, followed by western blotting. **(J)** Effects of WWP2 overexpression on ubiquitination of YBX1 in NSCLC cells. IB was performed with anti-ubiquitin (Ub) after cell lysates had been subjected to IP with YBX1 beads. Cells were treated with MG132 (20 μM, 5 h) before harvest. **(K)** SK-MES-1 cells were co-transfected with Flag-WWP2 or vector plasmids, along with Myc-Ub and its mutants (K48-linked and K63-linked

ubiquitin). Denaturing IP was performed, and the indicated proteins were detected by western blotting. **(L,M)** IB for YBX1 and WWP2 following IP with anti-WWP2 antibody in NSCLC cells with RP4-694A7.2 knockdown or overexpression. **(N)** Graphical illustration of regulation of YBX1 ubiquitination by RP4-694A7.2 and WWP2. Data are presented as the mean ± SD from three independent experiments, with significance determined by Student's *t*-test (***$P < 0.001$).

**Fig. 5.** RP4-694A7.2 promotes YBX1 nuclear import by strengthening the interaction of YBX1 with KPNA2. **(A,B)** Effects of RP4-694A7.2 knockdown or overexpression on nuclear import of YBX1, analyzed by western blotting using cytoplasmic (C) and nuclear (N) fractions from NSCLC cells. **(C,D)** Subcellular distribution of YBX1 assessed by IF in NSCLC cells following RP4-694A7.2 knockdown or overexpression; scale bar: 20 μm. **(E)** Colocalization analysis of YBX1 and KPNA2 in NSCLC cells by IF assay; scale bar: 20 μm. **(F)** Endogenous interaction between YBX1 and KPNA2 assessed by co-IP assay in NSCLC cells. **(G,H)** Specific association between RP4-694A7.2 and KPNA2 in NSCLC cells validated by RIP and RNA pull-down assays. **(I,J)** IB of YBX1 and KPNA2 following IP with anti-KPNA2 antibody in NSCLC cells with RP4-694A7.2 knockdown or overexpression. **(K)** Working model of RP4-694A7.2 enhancing KPNA2-mediated YBX1 nuclear import. Data are presented as the mean ± SD from three independent experiments, with significance determined by Student's

*t*-test (**$P < 0.01$, ***$P < 0.001$).

**Fig. 6.** RP4-694A7.2 promotes DEPDC1 transcription through YBX1 to drive NSCLC proliferation. **(A)** Heatmap and volcano plot of genes differentially expressed between RP4-694A7.2 knockdown and control cells. **(B)** Venn diagram showing the downstream genes coregulated by RP4-694A7.2 and YBX1. **(C,D)** RT-qPCR analysis of IGFBP3, DEPDC1, HHIP, CYP24A1 and FOS mRNA expression after RP4-694A7.2 or YBX1 knockdown in SK-MES-1 cells. **(E)** Correlation of DEPDC1 expression with RP4-694A7.2 or YBX1 expression in NSCLC according to GEPIA2 data. **(F)** Western blot analysis of DEPDC1 protein expression in NSCLC cells after RP4-694A7.2 knockdown or overexpression. **(G)** Western blot analysis of DEPDC1 protein expression in NSCLC cells after YBX1 knockdown or overexpression. **(H)** Representative western blot of DEPDC1 in SK-MES-1 cells with RP4-694A7.2 knockdown and YBX1 overexpression (left), and in NCI-H520 cells with RP4-694A7.2 overexpression and YBX1 knockdown (right). **(I)** YBX1-binding sites in the DEPDC1 promoter predicted using JASPAR. **(J)** Luciferase reporter assays measuring luciferase activity driven by the vector control, WT DEPDC1 promoter, or mutant promoters (Mut1: -TGTCCCATC-; Mut2: -TGTAACATC-) in HEK293T cells co-transfected with an HA-YBX1 plasmid. **(K)** Luciferase assays assessing *DEPDC1* promoter (WT, Mut1, Mut2) activity in NSCLC cells co-transfected with HA-YBX1 plasmids following RP4-694A7.2 knockdown or overexpression. **(L)** ChIP-qPCR analysis determining the

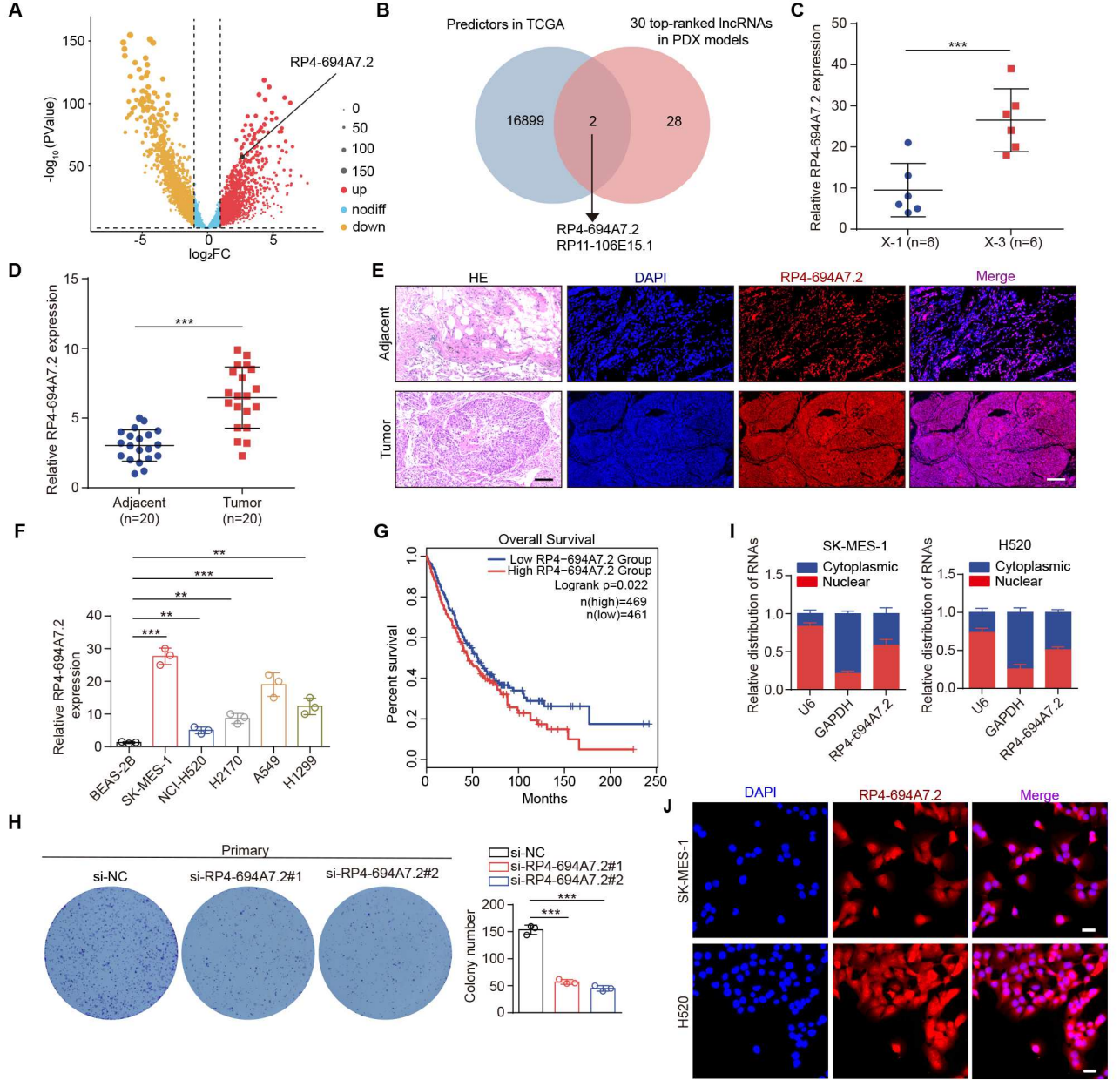
binding affinity of YBX1 to DEPDC1 promoter regions with RP4-694A7.2 knockdown or overexpression in NSCLC cells. ChIP-qPCR with IgG was used as a negative control. **(M,N)** Cell proliferation assessed by CCK-8 and colony formation assays in RP4-694A7.2-overexpressing NCI-H520 cells with or without DEPDC1 knockdown. **(O)** Model for RP4-694A7.2/YBX1-mediated transcriptional activation of *DEPDC1* in NSCLC. TSS, transcription start site. Data are presented as the mean ± SD from three independent experiments, with significance determined by Student's *t*-test (*$P$ < 0.05, **$P$ < 0.01, ***$P$ < 0.001; ns, not significant).

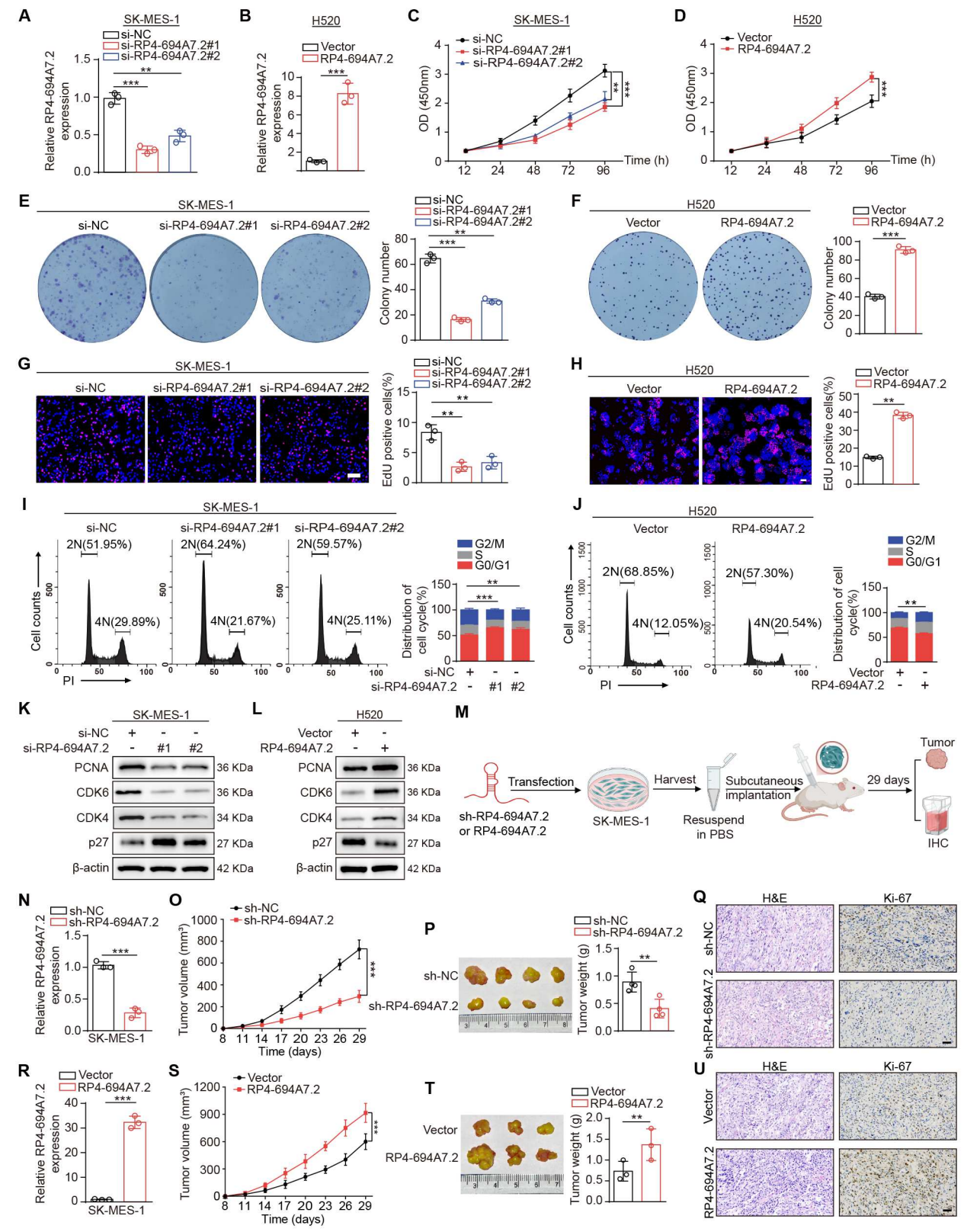
**Fig. 7.** RP4-694A7.2 promotes NSCLC proliferation by activating the Wnt/β-catenin pathway. **(A,B)** Gene ontology biological process enrichment and subsequent network-based cluster analysis showing that genes linked to RP4-694A7.2 are involved in the regulation of cell proliferation, apoptosis, and the cell cycle. **(C)** Kyoto Encyclopedia of Genes and Genomes enrichment analysis showing significantly enriched pathways after RP4-694A7.2 knockdown. **(D)** Gene set enrichment analysis indicating that reduced RP4-694A7.2 expression is correlated with suppression of Wnt/β-catenin signaling. **(E,F)** Western blot analysis of β-catenin, cyclin D1, and c-Myc protein levels in NSCLC cells with RP4-694A7.2 knockdown or overexpression. **(G,H)** Subcellular distribution of β-catenin in the cytoplasmic (C) and nuclear (N) fractions of NSCLC cells upon RP4-694A7.2 knockdown or overexpression, determined by

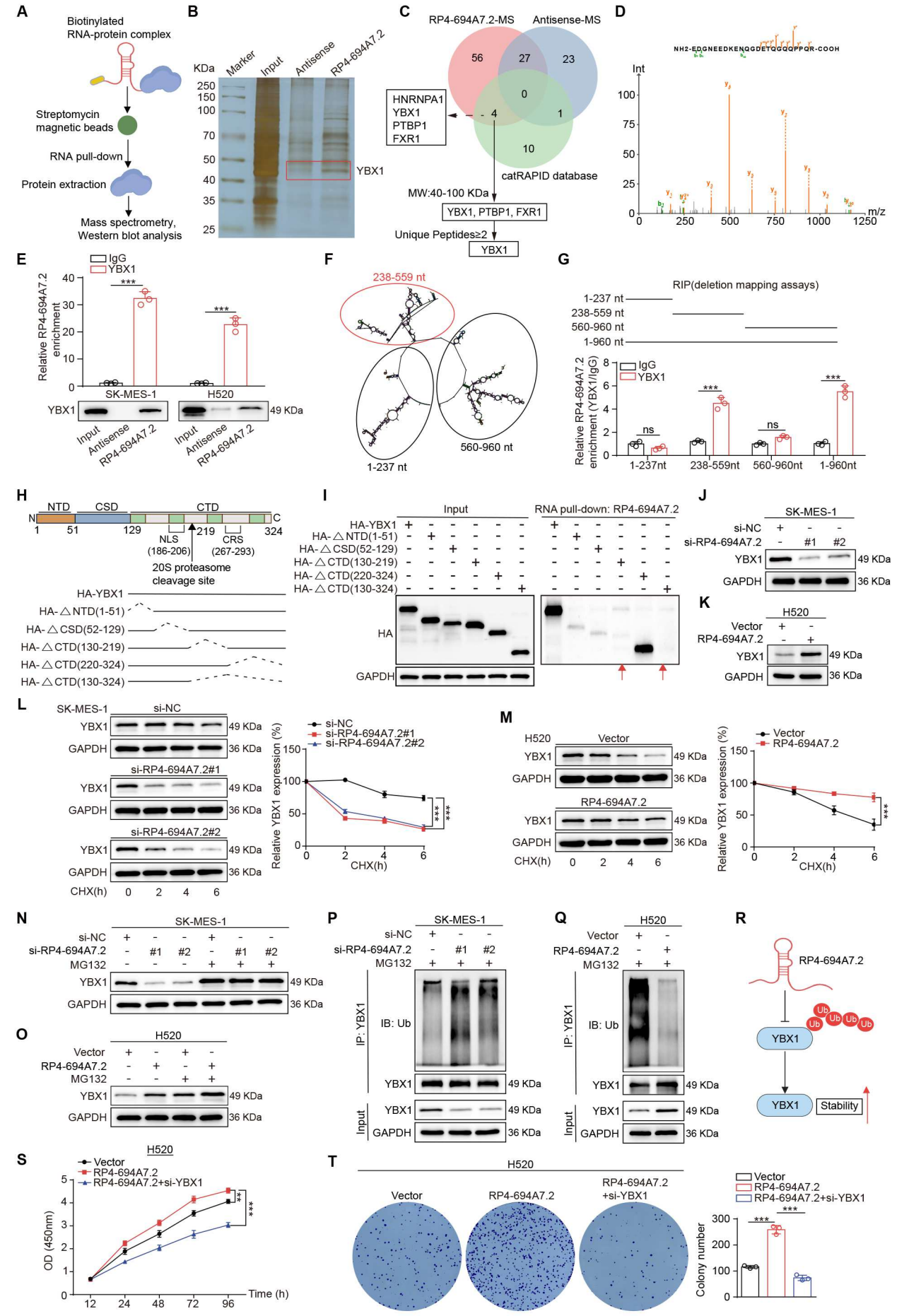
subcellular fractionation and western blotting. **(I,J)** TOP/FOP Flash assays showing Wnt/β-catenin pathway activity in NSCLC cells with RP4-694A7.2 knockdown or overexpression. **(K,L)** CCK-8 and colony formation assays assessing proliferation after β-catenin knockdown (si-β-catenin) or IWR-1 treatment (20 μM, 24 h) in RP4-694A7.2-overexpressing NCI-H520 cells. **(M)** Representative IHC images showing YBX1, DEPDC1, and β-catenin expression in xenograft tumors (from Fig. 2T). Scale bar: 50 μm. **(N)** Representative IHC staining of YBX1, DEPDC1, and β-catenin in paired NSCLC tissues and ANTs. Data are presented as the mean ± SD from three independent experiments, with significance determined by Student's *t*-test (***$P < 0.001$).

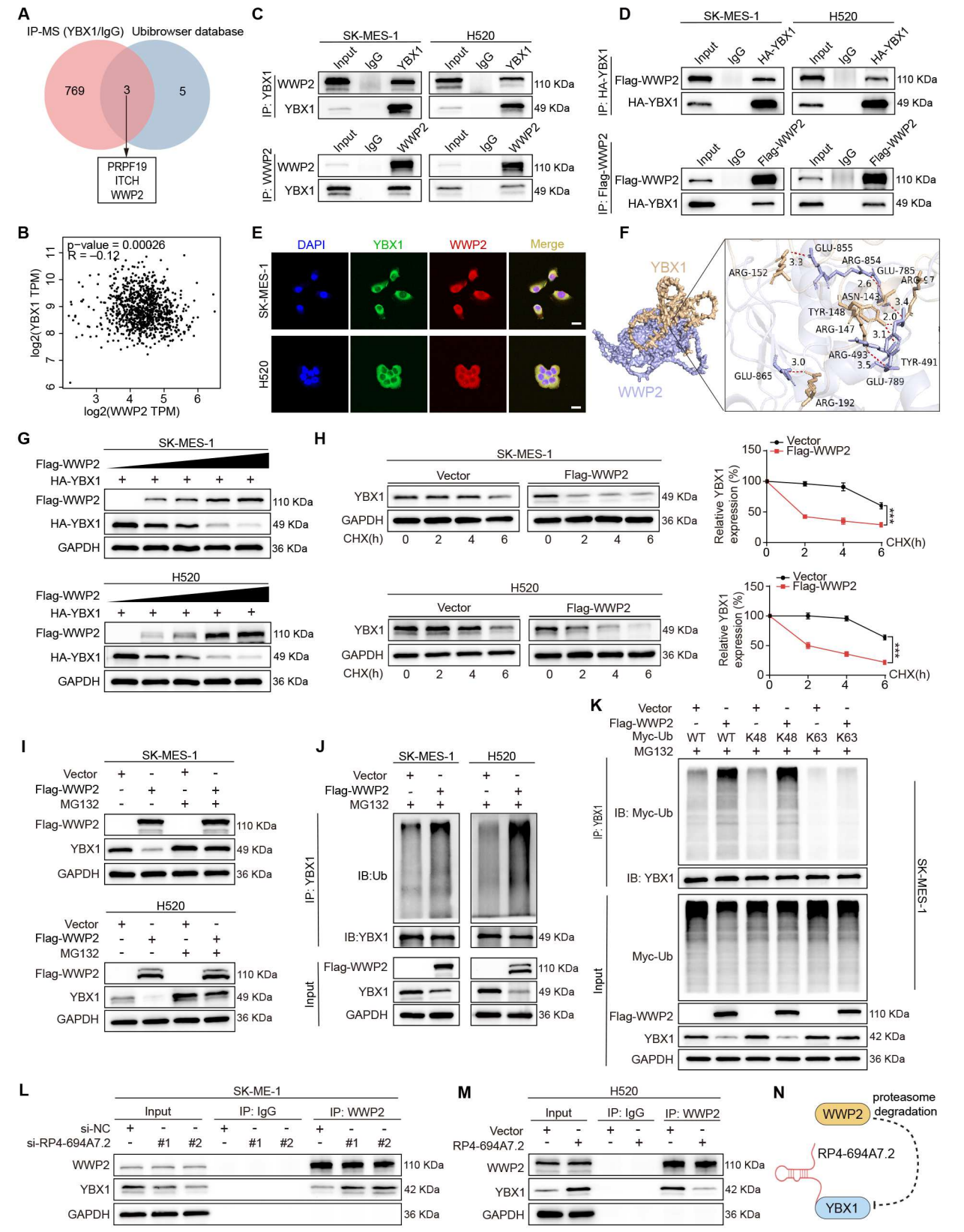
**Fig. 8.** RP4-694A7.2 knockdown suppresses tumor growth in NSCLC PDX models. **(A)** Schematic of the establishment of NSCLC PDX models. **(B)** Tumor growth curves for PDX mice in the blank, si-NC, and si-RP4-694A7.2 groups. PDX mice received intratumoral injection of siRNA (10 μg per tumor per dose) delivered with in vivo-jetPEI®, followed by tumor volume measurement every 3 days ($n = 5$ per group). **(C,D)** Representative tumor images and weights from each treatment group at 21 days post-injection. **(E)** RP4-694A7.2 knockdown efficiency in PDX mice was determined by RT-qPCR. **(F)** Mouse body weights were monitored every 3 days to assess systemic toxicity. **(G)** Representative images of H&E and IHC staining for Ki-67, YBX1, DEPDC1, and β-catenin in different PDX groups. Scale bars: 50 μm. **(H)** Schematic representation of the

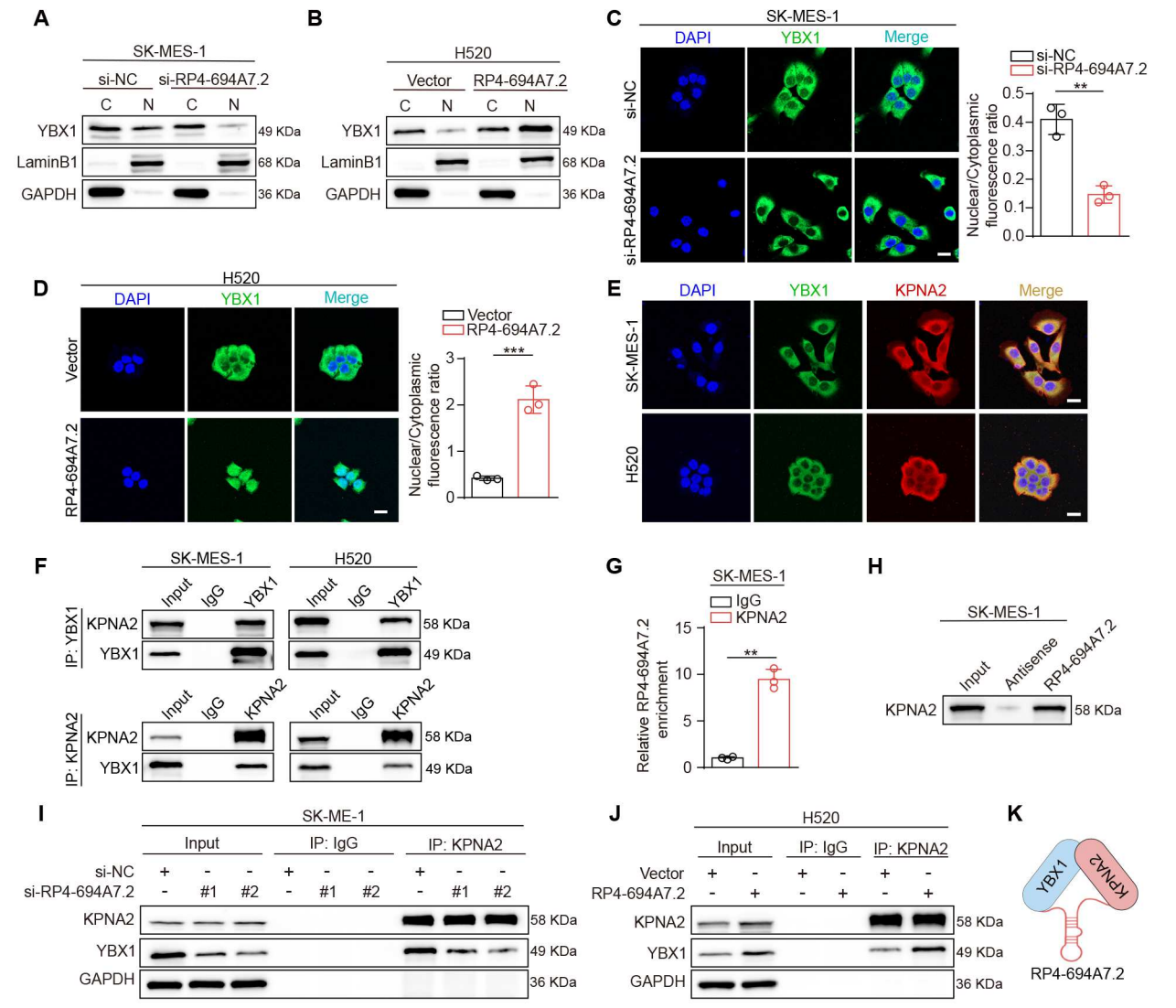
study. RP4-694A7.2 directly binds to YBX1, enhancing its stability by suppressing WWP2-mediated ubiquitination and proteasomal degradation. Moreover, RP4-694A7.2 promotes YBX1 nuclear import by strengthening the interaction of YBX1 with KPNA2. Nuclear-accumulated YBX1 subsequently binds to the *DEPDC1* promoter to facilitate *DEPDC1* transcription, leading to Wnt/β-catenin pathway activation and G1/S transition. Ultimately, this regulatory axis promotes NSCLC proliferation. TSS, transcription start site. Data are presented as the mean ± SD from three independent experiments, with significance determined by Student's *t*-test (**P* < 0.05, ****P* < 0.001; ns, not significant).

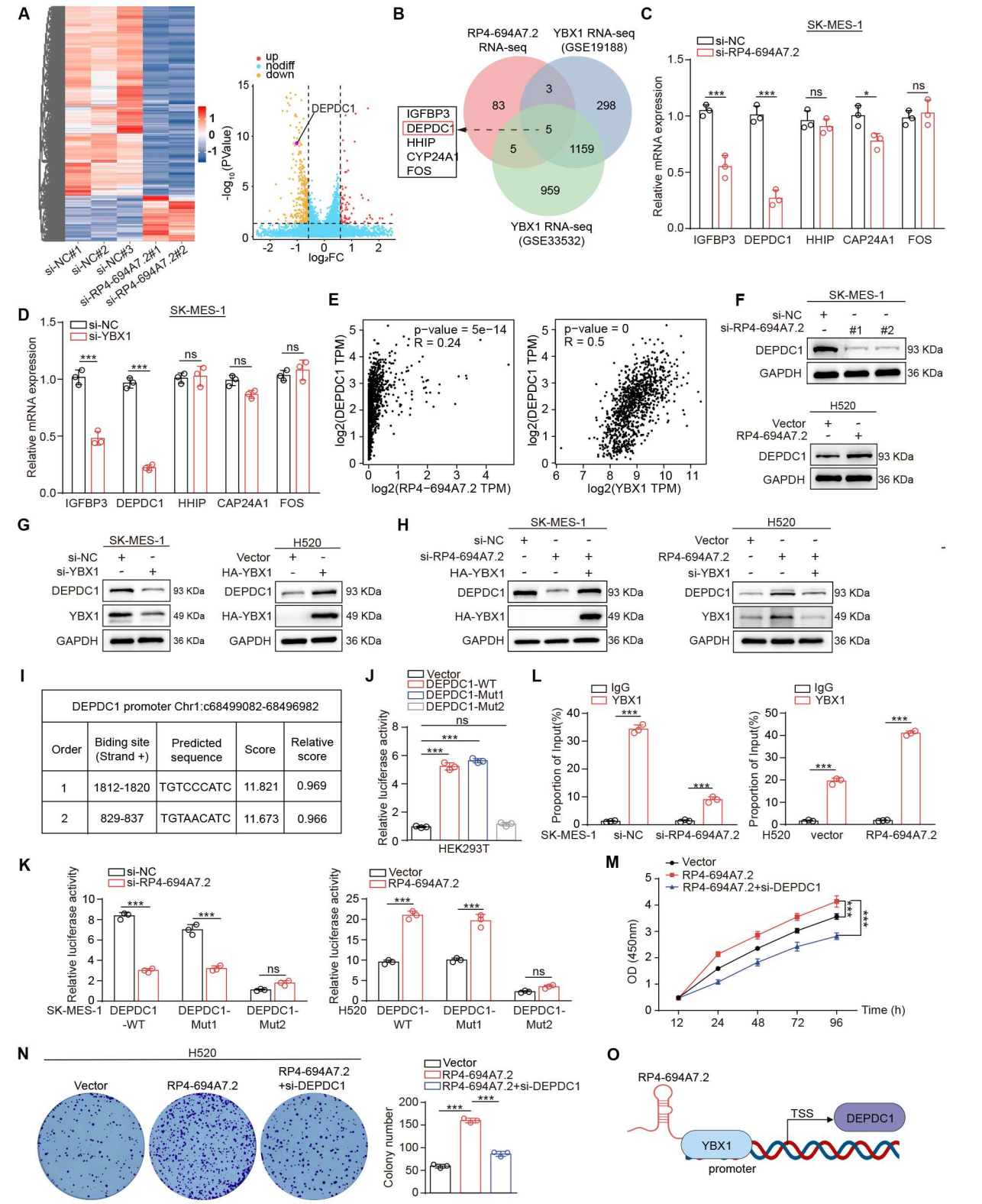

A
RP4-694A7.2
-log10(PValue)
log2FC
up
nodiff
down
B
Predictors in TCGA
30 top-ranked lncRNAs in PDX models
16899
2
28
RP4-694A7.2
RP11-106E15.1
C
Relative RP4-694A7.2 expression
X-1 (n=6)
X-3 (n=6)
D
Relative RP4-694A7.2 expression
Adjacent (n=20)
Tumor (n=20)
E
HE
DAPI
RP4-694A7.2
Merge
Adjacent
Tumor
F
Relative RP4-694A7.2 expression
BEAS-2B
SK-MES-1
NCI-H520
H2170
A549
H1299
G
Overall Survival
Low RP4-694A7.2 Group
High RP4-694A7.2 Group
Logrank p=0.022
n(high)=469
n(low)=461
Percent survival
Months
I
SK-MES-1
H520
Cytoplasmic
Nuclear
Relative distribution of RNAs
U6
GAPDH
RP4-694A7.2
H
Primary
si-NC
si-RP4-694A7.2#1
si-RP4-694A7.2#2
Colony number
J
DAPI
RP4-694A7.2
Merge
SK-MES-1
H520

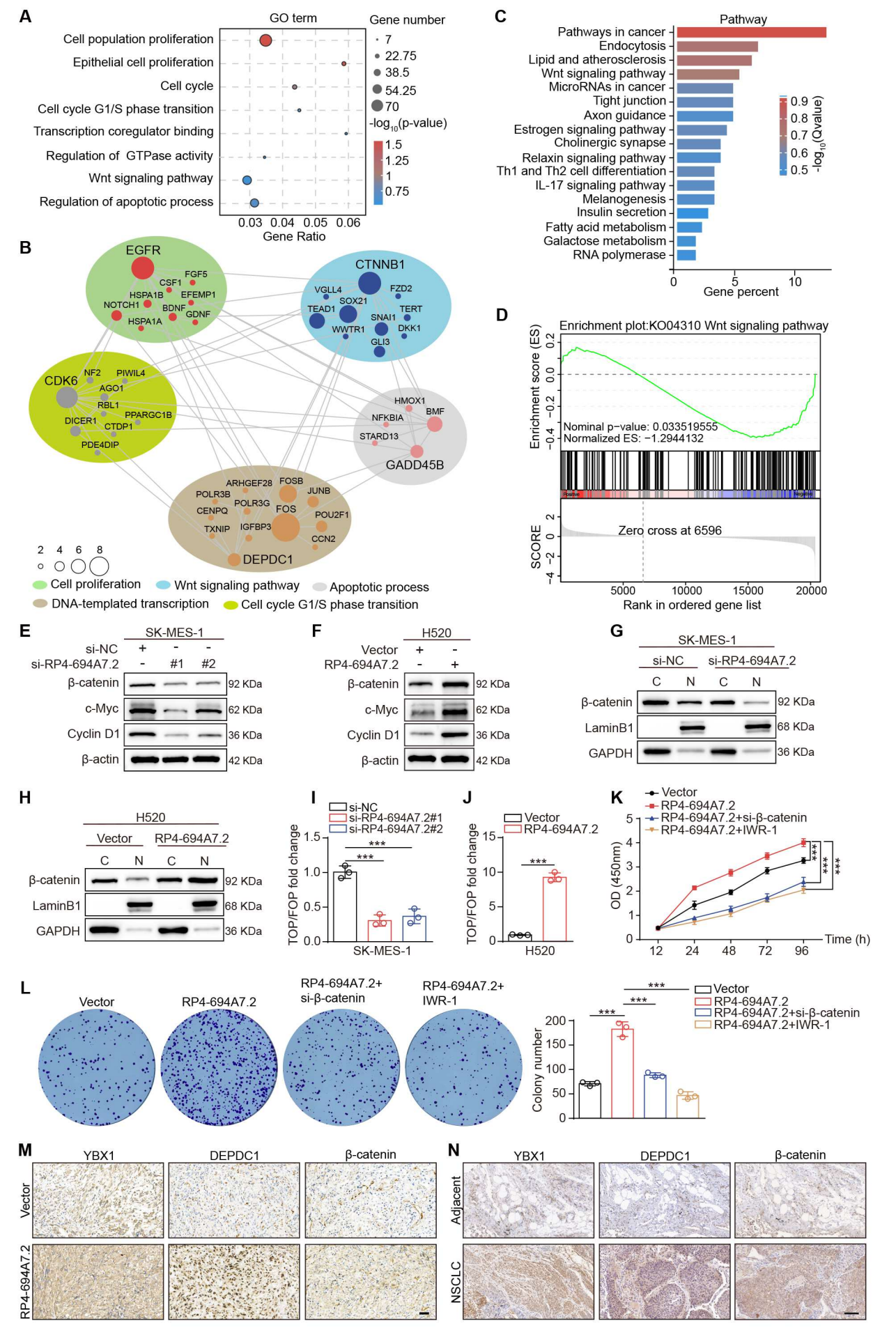

A
SK-MES-1
si-NC
si-RP4-694A7.2#1
si-RP4-694A7.2#2
Relative RP4-694A7.2 expression
B
H520
Vector
RP4-694A7.2
C
SK-MES-1
OD (450nm)
Time (h)
D
H520
E
SK-MES-1
Colony number
F
H520
G
SK-MES-1
EdU positive cells(%)
H
H520
I
SK-MES-1
Cell counts
PI
2N(51.95%)
4N(29.89%)
2N(64.24%)
4N(21.67%)
2N(59.57%)
4N(25.11%)
Distribution of cell cycle(%)
G2/M
S
G0/G1
J
H520
2N(68.85%)
4N(12.05%)
2N(57.30%)
4N(20.54%)
K
SK-MES-1
PCNA
CDK6
CDK4
p27
β-actin
36 KDa
34 KDa
27 KDa
42 KDa
L
H520
M
Transfection
sh-RP4-694A7.2
or RP4-694A7.2
SK-MES-1
Harvest
Resuspend
in PBS
Subcutaneous
implantation
29 days
Tumor
IHC
N
Relative RP4-694A7.2 expression
O
Tumor volume (mm³)
Time (days)
P
Tumor weight (g)
Q
H&E
Ki-67
R
S
T
U

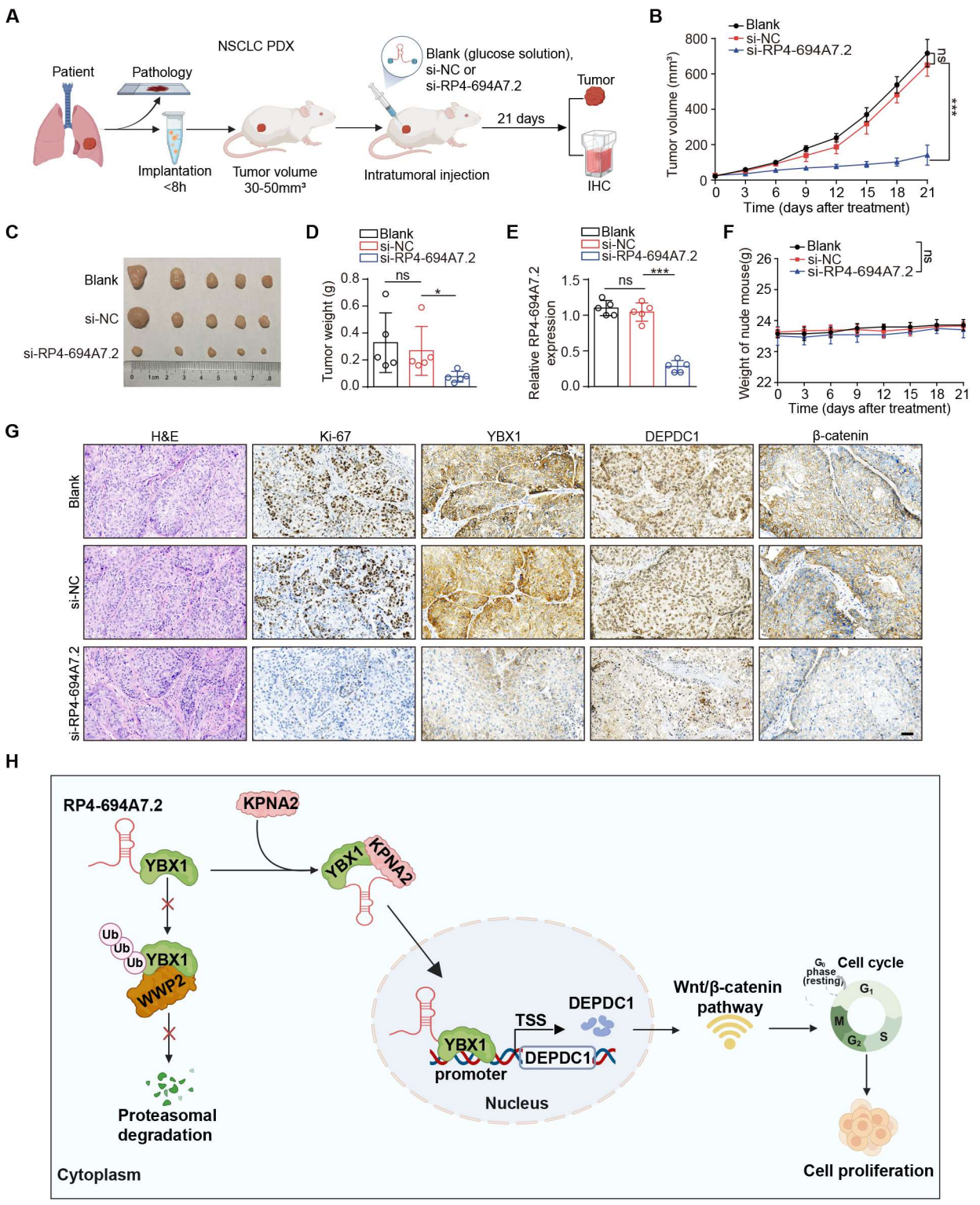

A
Biotinylated RNA-protein complex
Streptomycin magnetic beads
RNA pull-down
Protein extraction
Mass spectrometry, Western blot analysis
B
KDa
Marker
Input
Antisense
RP4-694A7.2
250
150
100
70
50
40
35
25
YBX1
C
RP4-694A7.2-MS
Antisense-MS
56
27
23
0
4
1
10
HNRNPA1
YBX1
PTBP1
FXR1
catRAPID database
MW:40-100 KDa
YBX1, PTBP1, FXR1
Unique Peptides≥2
YBX1
D
NH2-EDGNEEDKENQGDETQGQQPFQR-COOH
Int
m/z
E
IgG
YBX1
Relative RP4-694A7.2 enrichment
SK-MES-1
H520
YBX1
49 KDa
Input
Antisense
RP4-694A7.2
F
238-559 nt
560-960 nt
1-237 nt
G
RIP(deletion mapping assays)
1-237 nt
238-559 nt
560-960 nt
1-960 nt
IgG
YBX1
Relative RP4-694A7.2 enrichment (YBX1/IgG)
ns
1-237nt
238-559nt
560-960nt
1-960nt
H
NTD
CSD
CTD
N
C
1
51
129
219
324
NLS (186-206)
CRS (267-293)
20S proteasome cleavage site
HA-YBX1
HA-△NTD(1-51)
HA-△CSD(52-129)
HA-△CTD(130-219)
HA-△CTD(220-324)
HA-△CTD(130-324)
I
Input
RNA pull-down: RP4-694A7.2
HA
GAPDH
J
SK-MES-1
si-NC
si-RP4-694A7.2
#1
#2
YBX1
GAPDH
49 KDa
36 KDa
K
H520
Vector
RP4-694A7.2
L
SK-MES-1
si-NC
si-RP4-694A7.2#1
si-RP4-694A7.2#2
Relative YBX1 expression (%)
CHX(h)
M
H520
Vector
RP4-694A7.2
N
SK-MES-1
MG132
O
H520
P
SK-MES-1
IP: YBX1
IB: Ub
Input
Q
H520
R
RP4-694A7.2
Ub
YBX1
Stability
S
H520
Vector
RP4-694A7.2
RP4-694A7.2+si-YBX1
OD (450nm)
Time (h)
T
H520
Vector
RP4-694A7.2
RP4-694A7.2 +si-YBX1
Colony number


A
IP-MS (YBX1/IgG)
Ubibrowser database
769
3
5
PRPF19
ITCH
WWP2
B
p−value = 0.00026
R = −0.12
log2(YBX1 TPM)
log2(WWP2 TPM)
C
SK-MES-1
H520
Input
IgG
YBX1
WWP2
IP: YBX1
IP: WWP2
110 KDa
49 KDa
D
SK-MES-1
H520
IP: HA-YBX1
IP: Flag-WWP2
Flag-WWP2
HA-YBX1
E
DAPI
YBX1
WWP2
Merge
F
YBX1
WWP2
GLU-855
ARG-854
GLU-785
ARG-152
ASN-143
TYR-148
ARG-147
ARG-493
TYR-491
GLU-865
GLU-789
ARG-192
G
SK-MES-1
H520
Flag-WWP2
HA-YBX1
GAPDH
110 KDa
49 KDa
36 KDa
H
SK-MES-1
H520
Vector
Flag-WWP2
YBX1
GAPDH
CHX(h)
Relative YBX1 expression (%)
***
I
SK-MES-1
H520
Vector
Flag-WWP2
MG132
J
IP: YBX1
IB:Ub
IB:YBX1
Input
K
Vector
Flag-WWP2
Myc-Ub
WT
K48
K63
MG132
IP: YBX1
IB: Myc-Ub
IB: YBX1
Input
Myc-Ub
SK-MES-1
42 KDa
L
SK-ME-1
Input
IP: IgG
IP: WWP2
si-NC
si-RP4-694A7.2
WWP2
YBX1
GAPDH
M
H520
RP4-694A7.2
N
proteasome degradation
WWP2
RP4-694A7.2
YBX1


A
SK-MES-1
si-NC
si-RP4-694A7.2
C
N
C
N
YBX1
LaminB1
GAPDH
49 KDa
68 KDa
36 KDa
B
H520
Vector
RP4-694A7.2
C
N
C
N
YBX1
LaminB1
GAPDH
49 KDa
68 KDa
36 KDa
C
SK-MES-1
DAPI
YBX1
Merge
si-NC
si-RP4-694A7.2
si-NC
si-RP4-694A7.2
**
Nuclear/Cytoplasmic fluorescence ratio
0.5
0.4
0.3
0.2
0.1
0.0
D
H520
DAPI
YBX1
Merge
Vector
RP4-694A7.2
Vector
RP4-694A7.2
***
Nuclear/Cytoplasmic fluorescence ratio
3
2
1
0
E
DAPI
YBX1
KPNA2
Merge
SK-MES-1
H520
F
SK-MES-1
H520
Input
IgG
YBX1
Input
IgG
YBX1
IP: YBX1
KPNA2
YBX1
58 KDa
49 KDa
Input
IgG
KPNA2
Input
IgG
KPNA2
IP: KPNA2
KPNA2
YBX1
58 KDa
49 KDa
G
SK-MES-1
IgG
KPNA2
**
Relative RP4-694A7.2 enrichment
15
10
5
0
H
SK-MES-1
Input
Antisense
RP4-694A7.2
KPNA2
58 KDa
I
SK-ME-1
Input
IP: IgG
IP: KPNA2
si-NC
si-RP4-694A7.2
+
-
-
#1
#2
KPNA2
YBX1
GAPDH
58 KDa
49 KDa
36 KDa
J
H520
Input
IP: IgG
IP: KPNA2
Vector
RP4-694A7.2
+
-
KPNA2
YBX1
GAPDH
58 KDa
49 KDa
36 KDa
K
YBX1
KPNA2
RP4-694A7.2


A
si-NC#1
si-NC#2
si-NC#3
si-RP4-694A7.2#1
si-RP4-694A7.2#2
up
nodiff
down
DEPDC1
-log10 (PValue)
log2FC
B
RP4-694A7.2 RNA-seq
YBX1 RNA-seq (GSE19188)
YBX1 RNA-seq (GSE33532)
83
3
298
5
5
1159
959
IGFBP3
DEPDC1
HHIP
CYP24A1
FOS
C
SK-MES-1
si-NC
si-RP4-694A7.2
Relative mRNA expression
IGFBP3
DEPDC1
HHIP
CAP24A1
FOS
D
SK-MES-1
si-NC
si-YBX1
Relative mRNA expression
IGFBP3
DEPDC1
HHIP
CAP24A1
FOS
E
p−value = 5e−14
R = 0.24
log2(DEPDC1 TPM)
log2(RP4−694A7.2 TPM)
p−value = 0
R = 0.5
log2(YBX1 TPM)
F
SK-MES-1
si-NC
si-RP4-694A7.2
DEPDC1
GAPDH
93 KDa
36 KDa
H520
Vector
RP4-694A7.2
G
SK-MES-1
si-NC
si-YBX1
H520
Vector
HA-YBX1
DEPDC1
YBX1
GAPDH
93 KDa
49 KDa
36 KDa
H
SK-MES-1
si-NC
si-RP4-694A7.2
HA-YBX1
H520
Vector
RP4-694A7.2
si-YBX1
DEPDC1
YBX1
GAPDH
93 KDa
49 KDa
36 KDa
I
DEPDC1 promoter Chr1:c68499082-68496982
Order
Biding site (Strand +)
Predicted sequence
Score
Relative score
1
1812-1820
TGTCCCATC
11.821
0.969
2
829-837
TGTAACATC
11.673
0.966
J
Vector
DEPDC1-WT
DEPDC1-Mut1
DEPDC1-Mut2
Relative luciferase activity
HEK293T
L
IgG
YBX1
Proportion of Input(%)
SK-MES-1
si-NC
si-RP4-694A7.2
H520
vector
RP4-694A7.2
K
si-NC
si-RP4-694A7.2
Relative luciferase activity
SK-MES-1
DEPDC1 -WT
DEPDC1-Mut1
DEPDC1-Mut2
Vector
RP4-694A7.2
H520
M
Vector
RP4-694A7.2
RP4-694A7.2+si-DEPDC1
OD (450nm)
Time (h)
N
H520
Vector
RP4-694A7.2
RP4-694A7.2 +si-DEPDC1
Colony number
O
RP4-694A7.2
YBX1
promoter
TSS
DEPDC1


A
GO term
Gene number
Cell population proliferation
Epithelial cell proliferation
Cell cycle
Cell cycle G1/S phase transition
Transcription coregulator binding
Regulation of GTPase activity
Wnt signaling pathway
Regulation of apoptotic process
Gene Ratio
-log10(p-value)
B
EGFR
CTNNB1
CDK6
GADD45B
DEPDC1
Cell proliferation
Wnt signaling pathway
Apoptotic process
DNA-templated transcription
Cell cycle G1/S phase transition
C
Pathway
Pathways in cancer
Endocytosis
Lipid and atherosclerosis
Wnt signaling pathway
MicroRNAs in cancer
Tight junction
Axon guidance
Estrogen signaling pathway
Cholinergic synapse
Relaxin signaling pathway
Th1 and Th2 cell differentiation
IL-17 signaling pathway
Melanogenesis
Insulin secretion
Fatty acid metabolism
Galactose metabolism
RNA polymerase
-log10(Qvalue)
Gene percent
D
Enrichment plot:KO04310 Wnt signaling pathway
Enrichment score (ES)
Nominal p-value: 0.033519555
Normalized ES: −1.2944132
SCORE
Zero cross at 6596
Rank in ordered gene list
E
SK-MES-1
si-NC
si-RP4-694A7.2
β-catenin
c-Myc
Cyclin D1
β-actin
92 KDa
62 KDa
36 KDa
42 KDa
F
H520
Vector
RP4-694A7.2
G
SK-MES-1
si-NC
si-RP4-694A7.2
LaminB1
GAPDH
68 KDa
H
H520
Vector
RP4-694A7.2
I
si-NC
si-RP4-694A7.2#1
si-RP4-694A7.2#2
TOP/FOP fold change
SK-MES-1
J
Vector
RP4-694A7.2
H520
K
Vector
RP4-694A7.2
RP4-694A7.2+si-β-catenin
RP4-694A7.2+IWR-1
OD (450nm)
Time (h)
L
Vector
RP4-694A7.2
RP4-694A7.2+ si-β-catenin
RP4-694A7.2+ IWR-1
Colony number
M
YBX1
DEPDC1
β-catenin
Vector
RP4-694A7.2
N
YBX1
DEPDC1
β-catenin
Adjacent
NSCLC


A
NSCLC PDX
Patient
Pathology
Implantation
<8h
Tumor volume
30-50mm³
Blank (glucose solution),
si-NC or
si-RP4-694A7.2
Intratumoral injection
21 days
Tumor
IHC
B
Blank
si-NC
si-RP4-694A7.2
Tumor volume (mm³)
Time (days after treatment)
ns
***
C
Blank
si-NC
si-RP4-694A7.2
D
Blank
si-NC
si-RP4-694A7.2
Tumor weight (g)
ns
*
E
Blank
si-NC
si-RP4-694A7.2
Relative RP4-694A7.2 expression
ns
***
F
Blank
si-NC
si-RP4-694A7.2
Weight of nude mouse(g)
Time (days after treatment)
ns
G
H&E
Ki-67
YBX1
DEPDC1
β-catenin
Blank
si-NC
si-RP4-694A7.2
H
RP4-694A7.2
KPNA2
YBX1
YBX1
KPNA2
Ub
Ub
Ub
YBX1
WWP2
Proteasomal
degradation
Cytoplasm
YBX1
promoter
TSS
DEPDC1
DEPDC1
Nucleus
Wnt/β-catenin
pathway
Cell cycle
G0
phase
(resting)
G1
S
G2
M
Cell proliferation

## Supplementary Files

This is a list of supplementary files associated with this preprint. Click to download.

- SupplementaryFigures18.docx
- SupplementaryOriginalblots.pdf
- SupplementaryTables112.xlsx